

Orientation dynamics of small, triaxial–ellipsoidal particles in isotropic turbulence

Laurent Chevillard^{1,†} and Charles Meneveau²

¹Laboratoire de Physique de l'École Normale Supérieure de Lyon, CNRS, Université de Lyon, 46 allée d'Italie F-69007 Lyon, France

²Department of Mechanical Engineering and Center for Environmental and Applied Fluid Mechanics, The Johns Hopkins University, 3400 N. Charles Street, Baltimore, MD 21218, USA

(Received 22 May 2013; revised 19 September 2013; accepted 29 October 2013)

The orientation dynamics of small anisotropic tracer particles in turbulent flows is studied using direct numerical simulation (DNS) and results are compared with Lagrangian stochastic models. Generalizing earlier analysis for axisymmetric ellipsoidal particles (Parsa *et al.*, *Phys. Rev. Lett.*, vol. 109, 2012, 134501), we measure the orientation statistics and rotation rates of general, triaxial–ellipsoidal tracer particles using Lagrangian tracking in DNS of isotropic turbulence. Triaxial ellipsoids that are very long in one direction, very thin in another and of intermediate size in the third direction exhibit reduced rotation rates that are similar to those of rods in the ellipsoid's longest direction, while exhibiting increased rotation rates that are similar to those of axisymmetric discs in the thinnest direction. DNS results differ significantly from the case when the particle orientations are assumed to be statistically independent from the velocity gradient tensor. They are also different from predictions of a Gaussian process for the velocity gradient tensor, which does not provide realistic preferred vorticity–strain-rate tensor alignments. DNS results are also compared with a stochastic model for the velocity gradient tensor based on the recent fluid deformation approximation (RFDA). Unlike the Gaussian model, the stochastic model accurately predicts the reduction in rotation rate in the longest direction of triaxial ellipsoids since this direction aligns with the flow's vorticity, with its rotation perpendicular to the vorticity being reduced. For disc-like particles, or in directions perpendicular to the longest direction in triaxial particles, the model predicts noticeably smaller rotation rates than those observed in DNS, a behaviour that can be understood based on the probability of vorticity orientation with the most contracting strain-rate eigendirection in the model.

Key words: turbulent flows

1. Introduction

The fate of anisotropic particles in fluid flows is of considerable interest in the context of various applications, such as micro-organism locomotion (Pedley & Kessler 1992; Saintillan & Shelley 2007; Koch & Subramanian 2011), industrial manufacturing

† Email address for correspondence: laurent.chevillard@ens-lyon.fr

processes such as paper-making (Lundell, Soderberg & Alfredsson 2011), and natural phenomena such as ice crystal formation in clouds (Pinsky & Khain 1998). In many of these applications, the flow is highly turbulent and the rotational dynamics, alignment trends and correlations of anisotropic particles (such as fibres, discs or more general shapes) with the flow field become of considerable interest. For small tracer particles whose size is smaller than the Kolmogorov scale, the local flow around the particle can be considered to be inertia-free and Stokes flow solutions can be used to relate the rotational dynamics of the particles to the local velocity gradient tensor. This problem was considered in the classic paper by Jeffery (1922), who solved the problem of Stokes flow around a general triaxial–ellipsoidal object. He then derived, for the special case of an axisymmetric ellipsoid, the evolution equation for the orientation vector as function of the local velocity gradient tensor. Such dynamics lead to fascinating phenomena such as a rotation of rods when placed in a constant shear (Couette) flow and periodic motions on closed (Jeffery’s) orbits. The effects of such motions on the rheology of suspensions has been studied extensively, see e.g. Larson (1999).

In turbulent flows the velocity gradient tensor $A_{ij} = \partial u_i / \partial x_j$ fluctuates and is dominated by small-scale motions, of the order of the Kolmogorov scale η_K , and much work has focused on rod-like particles whose size is smaller than η_K . Studies of the orientation dynamics of such particles in turbulent flows have included those of Shin & Koch (2005) and Pumir & Wilkinson (2011) using isotropic turbulence data from direct numerical simulation (DNS), those of Zhang *et al.* (2001) and Mortensen *et al.* (2008) for particles in channel flow turbulence also using DNS, and those of Bernstein & Shapiro (1994) and Newsom & Bruce (1998) using data from laboratory and atmospheric measurements, respectively. (We remark that Shin & Koch (2005) also consider fibres that are longer than η_K). In numerical studies, Lagrangian tracking is most often used to determine the particle trajectories and simultaneous time integration of the Jeffery equation along the trajectory leads to predictions of the particles’ orientation dynamics.

Generic properties of the orientation dynamics, such as the variance of the fluctuating orientation vector or its alignment trends may also be studied by making certain assumptions about the Lagrangian evolution of the carrier fluid’s velocity gradient, in particular about its symmetric and antisymmetric parts, the strain-rate tensor $\mathbf{S} = (\mathbf{A} + \mathbf{A}^T)/2$ and rotation-rate tensor $\mathbf{\Omega} = (\mathbf{A} - \mathbf{A}^T)/2$. A number of recent theoretical studies have been based on the assumption that these flow variables obey isotropic Gaussian statistics, e.g. are the result of linear Ornstein–Uhlenbeck processes (see e.g. Brunk, Koch & Lion 1998; Pumir & Wilkinson 2011; Wilkinson & Kennard 2012; Vincenzi 2013). This assumption facilitates a number of theoretical results that may be used to gain insights into some features of the orientational dynamics, such as in the limiting case of strong vorticity with a weak random straining background, in which analytical solutions for the full probability density are possible (Vincenzi 2013). In these studies, the crucial role of alignments between the particles and the vorticity has been highlighted. As will be shown in the following, the relative alignment of the vorticity with the strain rate eigendirections, as first observed in Ashurst *et al.* (1987) is also crucially important.

In a recent study based on DNS of isotropic turbulence, Parsa *et al.* (2012) analyse the orientational dynamics of axisymmetric ellipsoids of any aspect ratio, that is, from rod-like shapes to spherical and disc-like shapes. They consider axisymmetric ellipsoids with major semi-axes of length d_1, d_2, d_3 , with $d_2 = d_3$. The unit orientation vector \mathbf{p} is taken to point in the direction of the axis of size d_1 . The parameter

$\alpha = d_1/d_2 = d_1/d_3$ describes uniquely the type of anisotropy: for $\alpha \rightarrow \infty$ one has rod or fibre-like particles with \mathbf{p} aligned with the axis, while for $\alpha \rightarrow 0$ one has discs with \mathbf{p} aligned perpendicular to the plane of the disc. For $\alpha \rightarrow 1$, one has spheres for which the choice of \mathbf{p} is arbitrary relative to the object's geometry. Parsa *et al.* (2012) report the variance and flatness factors of the orientation vector's rate of variation $\dot{\mathbf{p}}$ in time along fluid tracer trajectories. Strong dependencies of the variance as a function of α are observed. The trends differ significantly from results obtained when one assumes that \mathbf{p} and \mathbf{A} are uncorrelated, or that \mathbf{A} follows Gaussian statistics with no preferred vorticity–strain-rate alignments.

Both Shin & Koch (2005) and Parsa *et al.* (2012) observe that the non-trivial dependencies of the particle rotation variance as a function of α are associated with the alignment trends between flow vorticity and strain-rate eigenvectors. They remark that the orientation dynamics of anisotropic particles can thus serve as a useful diagnostic to examine the accuracy of Lagrangian models for the velocity gradient tensor in turbulence. Several Lagrangian stochastic models for the velocity gradient tensor in turbulence have been proposed in the literature (Girimaji & Pope 1990a; Cantwell 1992; Jeong & Girimaji 2003; Chertkov, Pumir & Shraiman 1999; Chevillard & Meneveau 2006; Naso, Pumir & Chertkov 2007; Biferale *et al.* 2007). As reviewed by Meneveau (2011), some of these models are for coarse-grained velocity gradients (Biferale *et al.* 2007) or tetrads of fluid particles (Chertkov *et al.* 1999; Naso *et al.* 2007), while others describe transient or quasi-steady state behaviour only (Cantwell 1992; Jeong & Girimaji 2003). To the best of the authors' knowledge, only two stochastic processes for the full velocity gradient tensor that includes realistic strain–vorticity correlations lead to stationary statistics. The first is due to Girimaji & Pope (1990a). It enforces by construction that the pseudo-dissipation is a lognormal process, and several additional free parameters must be prescribed. The second process is the recent fluid deformation approximation (RFDA) approach (Chevillard & Meneveau 2006) in which a physically motivated closure is used to model pressure Hessian and viscous effects. Recent interest has also focused on the fate of particles larger than η_K (see e.g. Zimmermann *et al.* 2011).

Here we shall focus on the case of inertia-free particles smaller than η_K , but of a general ellipsoidal shape that is not necessarily axisymmetric. The aims of the present work are twofold. First, to generalize the results of Parsa *et al.* (2012) to the case of generalized ellipsoidal particles, not restricted to the special case of bodies of revolution. For this purpose, we use a generalization of Jeffery's equation written in a convenient form by Junk & Illner (2007) that can be considered as a reformulation of earlier developments for triaxial–ellipsoidal particles by Jeffery (1922), Bretherton (1962), Gierszewski & Chaffey (1978), Hinch & Leal (1979) and Yarin, Gottlieb & Roisman (1997). The model, summarized in §2, describes the dynamics of all three orientation vectors pointing in each of the ellipsoid's major axes. The results depend upon two geometric parameters d_1/d_2 and d_1/d_3 that are equal for the axisymmetric cases. We aim to measure the variance and flatness of the rates of change of the three orientation vectors as a function of these two parameters. Also, geometric features such as the alignments between these orientation vectors and special local flow directions (vorticity and strain-rate eigendirections) will be reported. The results from analysis of DNS are presented in §3. The observed relative alignments highlight the importance of correlations among vorticity and strain-rate eigendirections in determining the particle orientation dynamics.

A second goal of this study, presented in §4, is to study the predictions of several models. As also done by Parsa *et al.* (2012) for axisymmetric particles, we first

consider predictions of the variance of particle rotation assuming the particle alignment is uncorrelated from the velocity gradient tensor. We also consider a Gaussian model of the velocity gradient tensor in which vorticity–strain-rate alignments are absent. Then we consider a stochastic model for the velocity gradient tensor (Chevillard & Meneveau 2006, 2007) in which pressure and viscous effects are modelled based on the RFDA. This model has been shown to yield realistic predictions of stationary statistics for the velocity gradient in turbulence at moderate Reynolds numbers (Chevillard *et al.* 2008). While the model has been generalized to passive scalars (Gonzalez 2009), rotating turbulence (Li 2011) and magnetohydrodynamic (MHD) turbulence (Hater, Homann & Grauer 2011), the fate of general triaxial–ellipsoidal anisotropic particles acted upon by a velocity gradient tensor that evolves according to the RFDA model has not yet been examined. The model results are compared with those from DNS and conclusions are presented in § 5.

2. Evolution equations for anisotropic particle orientation

Many numerical and theoretical studies use the Jeffery equation (Jeffery 1922) to predict the time evolution of the orientation of an axisymmetric ellipsoidal particle, as it is advected and acted on by a turbulent velocity field. Specifically, Jeffery’s equation for the unit orientation vector $\mathbf{p}(t)$ in the ellipsoid major axis of size d_1 (while $d_2 = d_3$ and $\alpha = d_1/d_2$) reads

$$\frac{d\mathbf{p}_n}{dt} = \Omega_{nj}p_j + \lambda(S_{nj}p_j - p_n p_k S_{kl}p_l), \quad (2.1)$$

where $\lambda = (\alpha^2 - 1)/(\alpha^2 + 1)$ and \mathbf{S} and Ω are the strain- and rotation-rate tensors, respectively. This equation is valid for axisymmetric ellipsoids in which two semi-axes are equal. The case of more general geometries was considered by Bretherton (1962) in which the linearity of Stokes flow and general symmetries gave the general form that any orientation evolution must have. Additional references dealing with the orientation dynamics of general ellipsoids include Gierszewski & Chaffey (1978), Hinch & Leal (1979) and Yarin *et al.* (1997). For instance, Hinch & Leal (1979) found that slight deviations from axisymmetry may cause significant variations in the resulting rates of particle rotation. In a recent paper (Junk & Illner 2007), the results were cast in a practically useful form, namely a system of three equations describing the evolution of three perpendicular unit vectors, each directed in one of the principal directions of the ellipsoid. Figure 1 illustrates the geometry of a general triaxial ellipsoid, exposed to the action of a surrounding local vorticity and strain-rate field at much larger scales. Since Stokes flow is assumed, the result is applicable only when the size of the tracer particle, i.e. its largest dimension, is smaller than the Kolmogorov scale of turbulence.

The Junk & Illner equation reads, for the three perpendicular unit vectors $\mathbf{p}^{(i)}$ ($i = 1, 2, 3$):

$$\frac{d\mathbf{p}^{(i)}}{dt} = \frac{1}{2}(\nabla \times \mathbf{u}) \times \mathbf{p}^{(i)} + \sum_{k,m} \epsilon_{ikm} \lambda^{(m)} \mathbf{p}^{(k)} \otimes \mathbf{p}^{(k)} \mathbf{S} \mathbf{p}^{(i)}, \quad (2.2)$$

where \otimes stands for the tensorial product, i.e. for any vectors \mathbf{u} and \mathbf{v} , we have $(\mathbf{u} \otimes \mathbf{v})_{ij} = u_i v_j$. Moreover, we sum over repeated subscript indices (i.e. Einstein convention), but we do not sum over repeated superscripts in parenthesis, unless

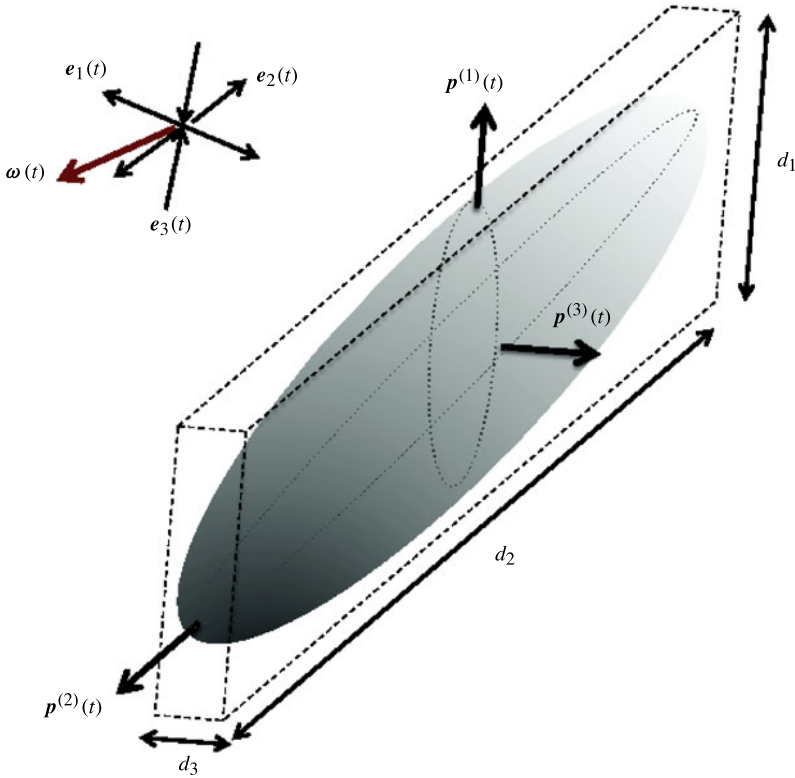


FIGURE 1. (Colour online) Sketch of triaxial-ellipsoidal particle with its three major axes scales d_1 , d_2 and d_3 , and its respective orientation unit vectors $\mathbf{p}^{(i)}$ for $i = 1, 2, 3$. Also shown are vorticity $\boldsymbol{\omega}$ and strain-rate eigenvectors (most extensional, \mathbf{e}_1 ; intermediate, \mathbf{e}_2 ; and most contracting, \mathbf{e}_3), characterizing the locally linear but time-dependent flow structure surrounding the particle.

explicitly stated. The $\lambda^{(m)}$ values are given by

$$\lambda^{(1)} = \frac{(d_2/d_3)^2 - 1}{(d_2/d_3)^2 + 1}, \quad \lambda^{(2)} = -\frac{(d_1/d_3)^2 - 1}{(d_1/d_3)^2 + 1}, \quad \lambda^{(3)} = \frac{(d_1/d_2)^2 - 1}{(d_1/d_2)^2 + 1}. \quad (2.3)$$

The $\lambda^{(m)}$ values are not independent. Solving (for example) for d_2/d_3 as a function of $\lambda^{(1)}$, one obtains $\lambda^{(1)} = 1/\lambda^{(2)} + 1/\lambda^{(3)}$. Then, in full index notation, the evolution equation reads

$$\frac{d\mathbf{p}_n^{(i)}}{dt} = \Omega_{nj}P_j^{(i)} + \sum_{k,m} \epsilon_{ikm} \lambda^{(m)} p_n^{(k)} p_q^{(k)} S_{ql} P_l^{(i)}. \quad (2.4)$$

The norm of $\mathbf{p}^{(i)}$ remains unity, since the inner product of the right-hand side of (2.2) by $\mathbf{p}^{(i)}$, or equivalently a contraction of the right-hand side of (2.4) with $p_n^{(i)}$, gives a contribution proportional to $p_n^{(i)} p_n^{(k)} = \delta_{ik}$. The $\sum_{k,m} \epsilon_{ikm}$ operation then makes this term vanish. We recall that for any vector \mathbf{u} , the quadratic form $\mathbf{u}^\top \boldsymbol{\Omega} \mathbf{u}$ vanishes if the tensor $\boldsymbol{\Omega}$ is antisymmetric. Also, Junk & Illner (2007) show that for the case of $d_2 = d_3$, i.e. $\lambda^{(1)} = 0$ and $\lambda^{(2)} = -\lambda^{(3)} = -\lambda$, one recovers the Jeffery equation: consider $i = 1$ as

the main axis. Then we have

$$\begin{aligned} \sum_{k,m} \epsilon_{1km} \lambda^{(m)} \mathbf{p}^{(k)} \otimes \mathbf{p}^{(k)} \mathbf{S} \mathbf{p}^{(i)} &= -\lambda^{(2)} \mathbf{p}^{(3)} \otimes \mathbf{p}^{(3)} \mathbf{S} \mathbf{p}^{(1)} + \lambda^{(3)} \mathbf{p}^{(2)} \otimes \mathbf{p}^{(2)} \mathbf{S} \mathbf{p}^{(1)} \\ &= \lambda (\mathbf{p}^{(3)} \otimes \mathbf{p}^{(3)} + \mathbf{p}^{(2)} \otimes \mathbf{p}^{(2)}) \mathbf{S} \mathbf{p}^{(1)}. \end{aligned} \quad (2.5)$$

Since the three unit vectors form an orthogonal basis, we can use the fact that

$$\mathbf{p}^{(1)} \otimes \mathbf{p}^{(1)} + \mathbf{p}^{(2)} \otimes \mathbf{p}^{(2)} + \mathbf{p}^{(3)} \otimes \mathbf{p}^{(3)} = \mathbf{I} \quad (2.6)$$

to obtain

$$\sum_{k,m} \epsilon_{1km} \lambda^{(m)} \mathbf{p}^{(k)} \otimes \mathbf{p}^{(k)} \mathbf{S} \mathbf{p}^{(i)} = \lambda (\mathbf{I} - \mathbf{p}^{(1)} \otimes \mathbf{p}^{(1)}) \mathbf{S} \mathbf{p}^{(1)}, \quad (2.7)$$

which is the last term in the Jeffery equation (equation (2.1)) taking $\mathbf{p}^{(1)} = \mathbf{p}$.

Under the assumption of small inertia-free particles, the ellipsoid's centroid follows the fluid flow. Therefore, the time evolution in (2.2) can be interpreted as the evolution along fluid particle trajectories and the time evolution of the orientations depends solely on the velocity gradient tensor. Knowing $\Omega_{ij}(t)$ and $S_{ij}(t)$ along fluid trajectories thus allows us to evaluate the Lagrangian evolution of particle orientations $\mathbf{p}^{(i)}$ by solving (2.2) (one may of course only solve for two components, since at all times, e.g. $\mathbf{p}^{(3)} = \mathbf{p}^{(1)} \times \mathbf{p}^{(2)}$).

In this article, we are interested in the variance of the rate of rotation of these orientation vectors (tumbling rates), extending the results for the variance of $\mathbf{p}^{(1)}$ when $d_2 = d_3$ and $d_1/d_2 \rightarrow +\infty$ (i.e. rods) studied by Shin & Koch (2005), and those of Parsa *et al.* (2012) for any d_1/d_2 with $d_2 = d_3$ (i.e. from rods to discs). Specifically, we are interested in the variance of the rotation speed of each direction vector as function of the two independent anisotropy parameters,

$$V^{(i)} \left(\frac{d_1}{d_2}, \frac{d_1}{d_3} \right) = \frac{1}{2 \langle \Omega_{rs} \Omega_{rs} \rangle} \langle \dot{\mathbf{p}}_n^{(i)} \dot{\mathbf{p}}_n^{(i)} \rangle \quad (2.8)$$

for the three orientation vectors $i = 1, 2, 3$, and we recall that no summation is assumed over superscripts (i). In (2.8), the average of the square norm $|\dot{\mathbf{p}}^{(i)}|^2$ is normalized by the average rate-of-rotation of the flow. We recall that for isotropic turbulence, $2 \langle \Omega_{rs} \Omega_{rs} \rangle = 2 \langle S_{rs} S_{rs} \rangle = \varepsilon/\nu$, where ε is the average dissipation per mass and ν the kinematic viscosity. Following Parsa *et al.* (2012) we are also interested in the flatness factor, namely

$$F^{(i)} \left(\frac{d_1}{d_2}, \frac{d_1}{d_3} \right) = \frac{\langle (\dot{\mathbf{p}}_n^{(i)} \dot{\mathbf{p}}_n^{(i)})^2 \rangle}{\langle \dot{\mathbf{p}}_r^{(i)} \dot{\mathbf{p}}_r^{(i)} \rangle^2}. \quad (2.9)$$

Further extending the prior analyses, we are also interested in the alignments between $\mathbf{p}^{(i)}$ and the vorticity and strain-rate eigenvectors in the flow.

3. Orientation dynamics of triaxial ellipsoids in DNS of isotropic turbulence

In this section, we consider orientation dynamics of triaxial ellipsoids in isotropic turbulence at moderate Reynolds number. We use results from DNS of forced isotropic turbulence at $R_\lambda \approx 125$ to provide Lagrangian time histories of the velocity gradient tensor $A_{ij}(t)$ along the tracer particle trajectories. These data are the same as those used by Chevillard & Meneveau (2011). The DNS is based on a pseudo-spectral method, de-aliased according to the 3/2 rule and with second-order accurate

Adams–Bashforth time stepping. The computational box is cubic (size 2π) with periodic boundary conditions in the three directions and a spatial mesh with 256^3 grid points. Statistical stationarity is maintained by an isotropic external force acting at low wavenumbers in order to ensure a constant power injection. It provides, in the units of the simulation, a constant energy injection rate of $\epsilon = 0.001$. The kinematic viscosity of the fluid is $\nu = 0.0004$. The Kolmogorov scale is $\eta_K = 0.016$ so that $\Delta x/\eta_K \approx 1.5$ (with $\Delta x = 2\pi/256$). Lagrangian trajectories are obtained using numerical integration of the fluid tracer equation. A second-order time integration scheme is used (involving both velocity and acceleration at the current spatial location), with a time step $\Delta t = 3.5 \times 10^{-3}$ and cubic spatial interpolation in the three spatial directions to obtain velocity and acceleration at particle locations. A total of 512 such trajectories, of length of order of 15 large-eddy turnover times, is used in this study, with initial positions chosen at random in the flow volume. We have tested for statistical convergence levels using fewer and shorter trajectories (data not shown) and obtained results with negligible deviations from those plotted. Statistical quantities shown, including the flatness, have converged statistically to levels equal to or smaller than the amplitudes of the deviations from smooth behaviour shown in the plots (i.e. better than $\sim 3\%$). Once we have the Lagrangian time history of the velocity gradient tensor $\mathbf{A}(t)$, we integrate numerically the dynamics of the three vectors $\mathbf{p}^{(i)}$ starting from three unit vectors that point in arbitrary (randomly chosen) initial directions, constrained by the orthonormality condition $p_q^{(i)}(0) = \delta_{iq}$. For high accuracy (e.g. always checking that the set of three vectors remains orthonormal), we integrate (2.2) using a standard fourth-order Runge–Kutta method, using the same time step as used in the time integration to obtain the time history of $\mathbf{A}(t)$.

3.1. Variance and flatness of the time derivative of orientation vectors

We focus in this section on the variance $V^{(i)}(d_1/d_2, d_1/d_3)$ of the orientation vectors as defined in (2.8). The sketch in figure 2 represents the various limiting geometries and orientation vectors as function of the ratios d_1/d_2 and d_1/d_3 . Owing to the symmetries inherent in the labelling of the various directions, interchanging d_2 and d_3 while leaving d_1 unchanged should not affect the rotation rates in the $i = 1$ direction. Hence, the results are expected to be symmetric around the 45° line ($d_1/d_2 = d_1/d_3$), i.e.

$$V^{(1)}\left(\frac{d_1}{d_2}, \frac{d_1}{d_3}\right) = V^{(1)}\left(\frac{d_1}{d_3}, \frac{d_1}{d_2}\right). \quad (3.1)$$

Also, since upon interchanging the two directions (2) and (3), the corresponding direction vector must be interchanged, we expect

$$V^{(3)}\left(\frac{d_1}{d_3}, \frac{d_1}{d_2}\right) = V^{(2)}\left(\frac{d_1}{d_2}, \frac{d_1}{d_3}\right), \quad (3.2)$$

and hence only results for $V^{(1)}$ and $V^{(2)}$ are presented. The same symmetries apply to the flatness factor, and hence only results for $F^{(1)}$ and $F^{(2)}$ are presented.

In figure 3 we show the normalized variance as function of the two ratios of semi-axes length, obtained from DNS. Several observations may be made based on these results. First, for axisymmetric ellipsoids along the $d_1/d_3 = d_1/d_2$ line, the results for $V^{(1)}$ agree with those of Parsa *et al.* (2012). Namely, for fibre-like ellipsoids ($d_1/d_2 \rightarrow \infty$), the normalized variance tends to values near 0.09, whereas for disc-like ellipsoids, it tends to values near 0.24. For spherical particles, it is near 0.17. The trend at the edges of the negative 45° line, $d_1/d_3 = (d_1/d_2)^{-1}$ represent particles

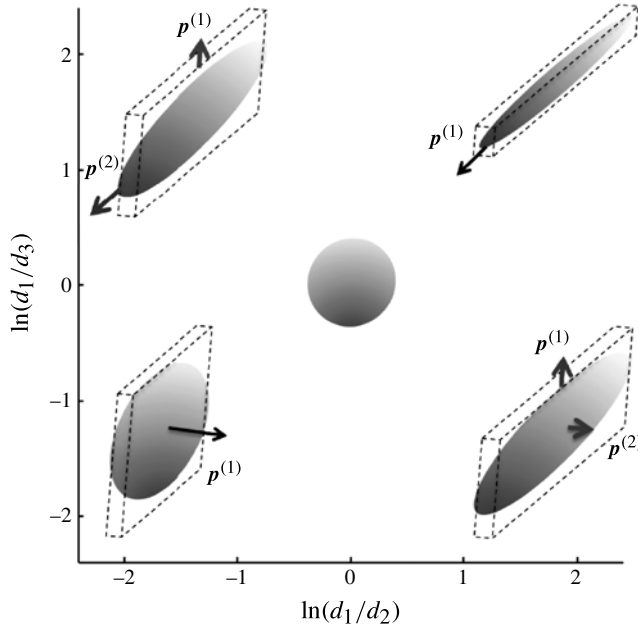


FIGURE 2. Sketch of triaxial ellipsoid geometries and orientation vectors, as function of semi-axes ratios d_1/d_2 and d_1/d_3 .

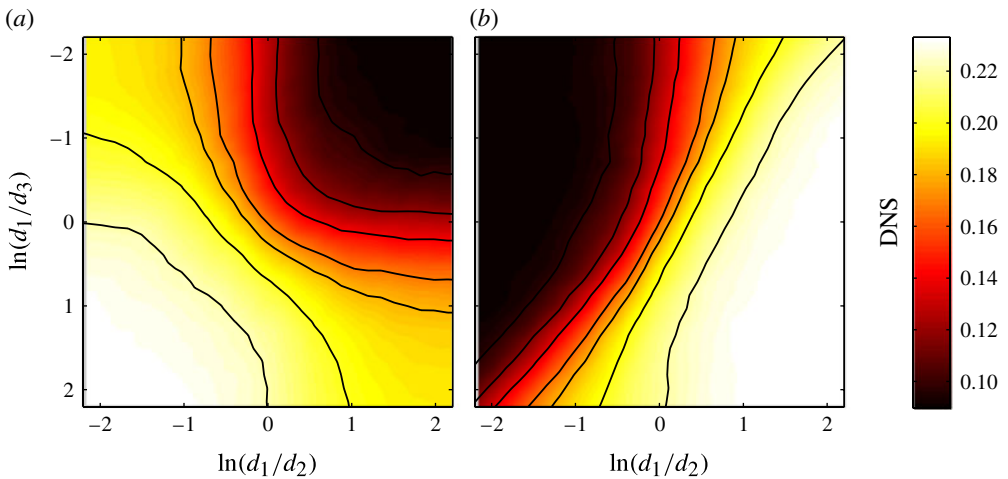


FIGURE 3. (Colour online) Variance of rate-of-change of two ellipsoid orientation vectors \mathbf{p}^1 and \mathbf{p}^2 as function of the two ratios of semi-axes length, obtained from DNS. Contour lines go from 0.1 to 0.22 separated by 0.02: (a) $V^{(1)}$; (b) $V^{(2)}$.

that are long in one direction (e.g. $d_2 \gg d_1$), very thin in another ($d_3 \ll d_1$) and of intermediate size (d_1) in the direction chosen for $\mathbf{p}^{(1)}$. As can be seen, $V^{(1)}$ along this line remains near the spherical value, with a small increase towards $V^{(1)}(d_1/d_2 \rightarrow 0, d_1/d_3 \rightarrow \infty) \sim 0.19$.

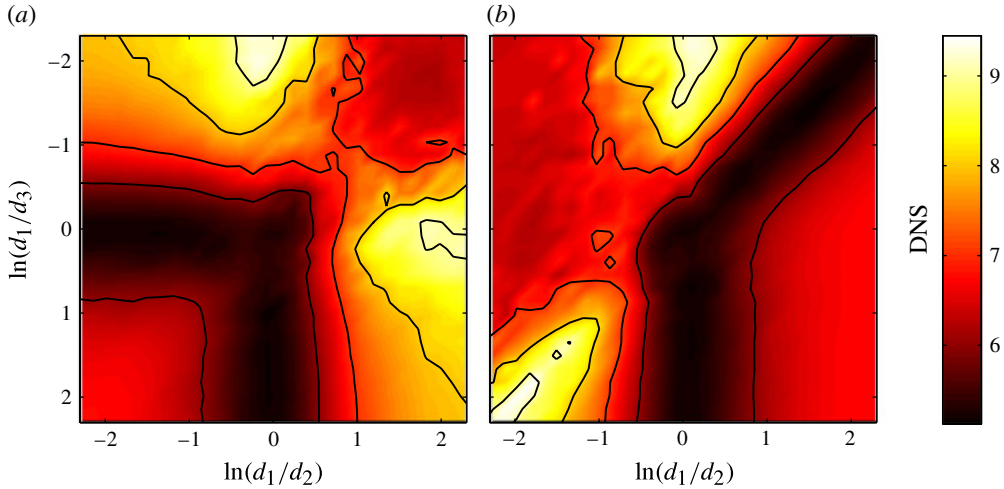


FIGURE 4. (Colour online) Flatness of rate-of-change of two ellipsoid orientation vectors $\mathbf{p}^{(1)}$ and $\mathbf{p}^{(2)}$ as function of the two ratios of semi-axes length, obtained from DNS. Contour lines correspond to flatness values of 2.1, 2.2, 3, 3.8, 5, 6, 7, 8, 9: (a) $F^{(1)}$; (b) $F^{(2)}$.

The variance $V^{(2)}$ of the orientation vector in a direction perpendicular to $\mathbf{p}^{(1)}$ and along the direction of either the longest or shortest ellipsoid axis exhibits significant dependence upon the semi-axes scale ratios. For $\mathbf{p}^{(2)}$ aligned along the largest ellipsoid semi-axis (figure 3a), the variance is reduced, to about 0.09. This is similar to the variance for long axisymmetric fibres. For $\mathbf{p}^{(2)}$ aligned along the shortest ellipsoid semi-axis (figure 3b), the variance is large, of the order of 0.24, similar to the values for axisymmetric discs. It was noted by Parsa *et al.* (2012) that the transition between rod and disc-like behaviours occurred quite rapidly, with aspect ratios of about $d_1/d_2 \sim 2-3$ already showing results quite close to the asymptotic values. As can be seen in the results for $V^{(2)}$, the transition is even more rapid along the negative 45° , $d_1/d_3 = (d_1/d_2)^{-1}$ line, where most of the change in variance occurs for values between $d_1/d_2 \sim 0.6$ and 1.6.

Next, the flatness factors of the orientation rates-of-change, $F^{(1)}$ and $F^{(2)}$ (equation (2.9)) are presented, in figure 4. As found by Parsa *et al.* (2012) for axisymmetric cases, the flatness is in a range between 5 and 10. These values are clearly above $5/3$, which is the value obtained when the vector $\dot{\mathbf{p}}^{(1)}$ is assumed to have zero-average independent Gaussian components (Parsa *et al.* 2012) or 2, which is the value obtained for spheres (i.e. $d_1 = d_2 = d_3$) when $\dot{\mathbf{p}}^{(1)}$ is assumed independent from velocity gradients, themselves assumed Gaussian (see Appendix and (A 15)). The maximum flatness is observed near the top middle and right middle regions, where $d_1 \approx d_2$ and $d_3 \ll d_1$ or $d_1 \approx d_3$ and $d_1 \approx d_2$, respectively, i.e. disc-like shapes, but with $\mathbf{p}^{(1)}$ aligned in the plane of the disc. These were cases where the variance is relatively small (see figure 3). For $F^{(2)}$, the structure is more complex, but the limiting cases showing peak flatness values are consistent with the results for $F^{(1)}$: namely the peaks occur for disc-like shapes with the orientation vector aligned in the plane of the disc. Consistent with the values of flatness that significantly exceed the Gaussian value and equivalent to the results of Parsa *et al.* (2012), the probability density functions (p.d.f.s) of $\dot{p}_n^{(i)} \dot{p}_n^{(i)}$ show elongated tails (data not shown).

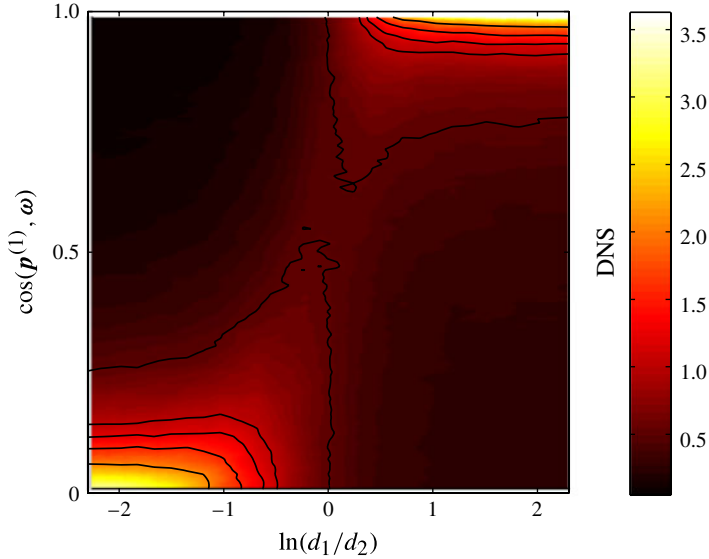


FIGURE 5. (Colour online) P.d.f. of the cosine of the angle between the vorticity direction $\hat{\omega}$ and the ellipsoid's major axis $\mathbf{p}^{(1)}$ for axisymmetric case (i.e. $d_2 = d_3$), as a function of the anisotropy parameter d_1/d_2 , obtained from DNS. Contour lines correspond to p.d.f. values of 0.5, 1, 1.2, 1.5, 2.

3.2. Alignments of orientation vectors with vorticity and strain eigenframe

Next, we consider the alignment trends of particle orientation with respect to the vorticity and strain-rate tensor's eigendirections. For this discussion, we focus on the case of axisymmetric particles and hence focus only on the single orientation vector $\mathbf{p}^{(1)}$. Alignment trends with vorticity are quantified by measuring the p.d.f. of $\cos(\theta_{p^{(1)}\omega}) = \mathbf{p}^{(1)} \cdot \hat{\omega}$ of the angle between $\mathbf{p}^{(1)}$ and the vorticity direction $\hat{\omega} = \boldsymbol{\omega}/|\boldsymbol{\omega}|$. Results are shown in figure 5 as a function of the parameter $\alpha = d_1/d_2$.

As can be seen, for fibre or rod-like particles ($d_1/d_2 \rightarrow \infty$), the results confirm strong alignment with vorticity, a well-known trend found in many prior studies of alignments of line elements in turbulence (Girimaji & Pope 1990b; Shin & Koch 2005; Pumir & Wilkinson 2011). In the other limit, for disc-like particles, the results show that $\mathbf{p}^{(1)}$ is more preferentially perpendicular to the vorticity. That is to say, the vorticity tends to be in the plane of the disc. These orientation trends help understand the parameter dependencies seen in the variance of $\dot{\mathbf{p}}^{(1)}$, i.e. $V^{(1)}$ shown in figure 3. Specifically, along the diagonal $d_1/d_2 = d_1/d_3$ for long rods (i.e. $d_1/d_2 \rightarrow \infty$), the particle rotates along its axis of symmetry since $\mathbf{p}^{(1)}$ is preferentially aligned with the vorticity. This leads to a reduced level of fluctuations $V^{(1)}$ (Shin & Koch 2005; Parsa *et al.* 2012). For discs, i.e. $d_1/d_2 \rightarrow 0$, the vorticity is preferentially aligned in the plane of the disc which, like a spinning coin on a table, implies faster rotation of the orientation vector perpendicular to that plane.

A similar analysis is done for alignments with each of the strain-rate eigendirections. The alignments of $\mathbf{p}^{(1)}$ with each of the strain-rate eigenvectors are quantified using the p.d.f. of the respective angle cosines. The results are shown in figure 6. The strongest alignment trend observed from the DNS is for disc-like particles to align with the most contracting eigendirection (figure 6c). This trend is quite easy to understand intuitively: the disc-plane tends to become perpendicular to the incoming (contracting) relative

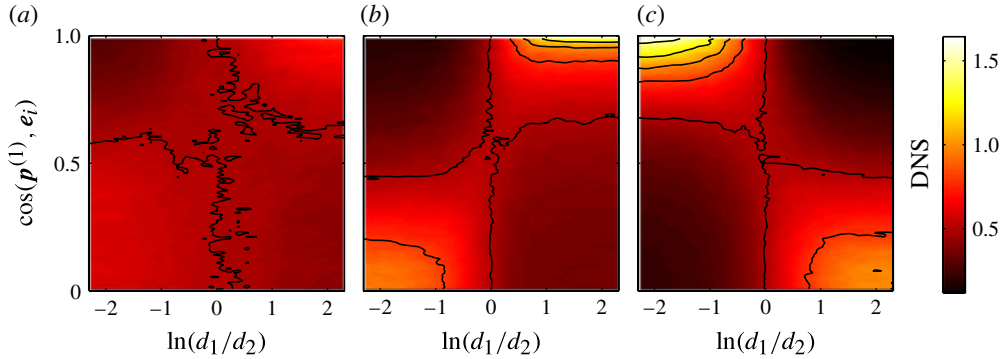


FIGURE 6. (Colour online) P.d.f. of cosine of angle between the strain-rate tensor eigendirections e_i and the axisymmetric ellipsoid's major axis $\mathbf{p}^{(1)}$ for axisymmetric case, as function of the anisotropy parameter $d_1/d_2 = d_1/d_3$, obtained from DNS. Here e_1 is the direction of strongest extension (i.e. most positive eigenvalue), whereas e_3 is the direction of strongest contraction (i.e. most negative eigenvalue). Contour lines correspond to p.d.f. values of 0.5, 0.8, 1, 1.2, 1.5: (a) p.d.f. $\cos(\mathbf{p}^{(1)}, e_1)$; (b) p.d.f. $\cos(\mathbf{p}^{(1)}, e_2)$; (c) p.d.f. $\cos(\mathbf{p}^{(1)}, e_3)$.

local flow direction. In addition, recall that the vorticity is perpendicular to the most contracting direction (data not shown, see Meneveau (2011)). The other trend that is visible is that rod-like particles tend to become perpendicular to the most contracting direction. This trend is consistent with its alignment with the vorticity, which tends to be perpendicular to the most contractive direction. As observed previously, rod-like particles tend to align well with the intermediate eigenvectors, while disc-like particles show preponderance of perpendicular orientation with regards to the intermediate eigenvector. Interestingly, alignment with the most stretching eigendirection appears to be very weak, almost random.

In order to examine alignment trends in non-axisymmetric cases, we consider the case along the negative 45° diagonal $d_1/d_3 = (d_1/d_2)^{-1}$. According to figure 3(b) along this line there are very strong variations of the rotation rate variance of $\mathbf{p}^{(2)}$, specifically with very large variance when $d_1/d_2 \gg 1$ and $d_1/d_3 \ll 1$ (bottom right corner). This is the rate of rotation of the vector aligned in the direction of the smallest of the three semi-axes (d_2). To explain these trends it is of interest to consider the orientation statistics of the vector $\mathbf{p}^{(2)}$ with respect to vorticity and strain-rate eigendirections, along the $d_1/d_3 = (d_1/d_2)^{-1}$ line. The results are presented in figures 7 and 8. Very similar results are obtained as in figures 5 and 6. Namely, when fluctuations of rotation rate of $\mathbf{p}^{(2)}$ are seen to be high, e.g. near $d_1/d_3 = (d_1/d_2)^{-1} \rightarrow 0$, this is accompanied by $\mathbf{p}^{(2)}$ being preferentially orthogonal to the vorticity direction. Conversely, when fluctuations are lower, e.g. when $d_1/d_3 = (d_1/d_2)^{-1} \rightarrow \infty$, one sees that $\mathbf{p}^{(2)}$ and the vorticity are preferentially aligned.

4. Predictions from stochastic models

4.1. Statistically independent orientations and velocity gradient tensor

First, we consider the case when the particle orientation vectors $\mathbf{p}^{(i)}$ and the velocity gradient tensor \mathbf{A} are assumed to be statistically independent, as proposed by Shin & Koch (2005). A similar analysis has been presented for axisymmetric particles by Parsa *et al.* (2012), leading to the following result for the variance of the rotation rate

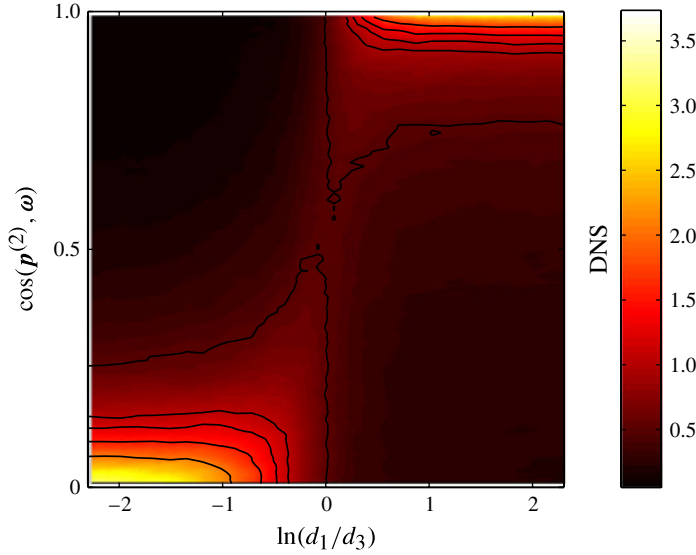


FIGURE 7. (Colour online) P.d.f. of cosine of angle between the vorticity direction $\hat{\omega}$ and the ellipsoid's second semi-axis $\mathbf{p}^{(2)}$, as function of the anisotropy parameters $d_1/d_3 = (d_1/d_2)^{-1}$, obtained from DNS. Contour lines correspond to p.d.f. values of 0.5, 1, 1.2, 1.5, 2.

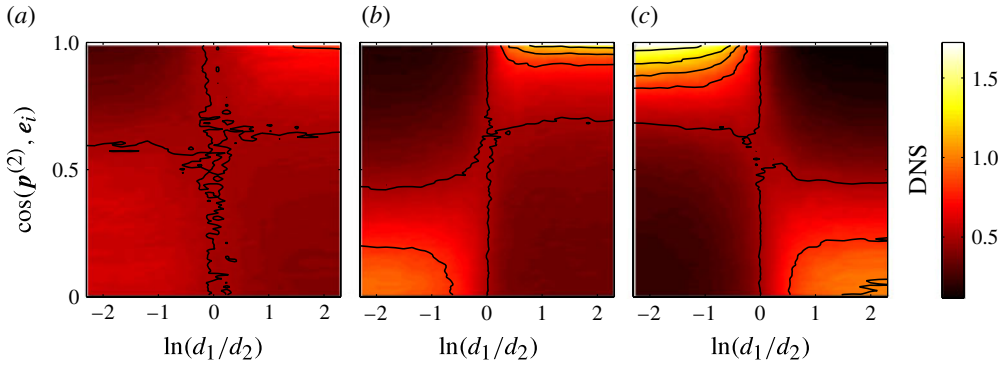


FIGURE 8. (Colour online) P.d.f. of cosine of angle between the strain-rate tensor eigendirections \mathbf{e}_i and the ellipsoid's second semi-axis $\mathbf{p}^{(2)}$, as function of the anisotropy parameter d_1/d_2 , choosing $d_1/d_3 = (d_1/d_2)^{-1}$, obtained from DNS. Contour lines correspond to p.d.f. values of 0.5, 0.8, 1, 1.2, 1.5: (a) p.d.f. $\cos(\mathbf{p}^{(2)}, \mathbf{e}_1)$; (b) p.d.f. $\cos(\mathbf{p}^{(2)}, \mathbf{e}_2)$; (c) p.d.f. $\cos(\mathbf{p}^{(2)}, \mathbf{e}_3)$.

of the orientation vector:

$$\frac{\langle \dot{p}_n \dot{p}_n \rangle_{SI}}{2 \langle \Omega_{rs} \Omega_{rs} \rangle} = \frac{1}{6} + \frac{1}{10} \lambda^2, \quad (4.1)$$

where SI stands for statistically independent and, as before, the vector \mathbf{p} coincides with $\mathbf{p}^{(1)}$, and $\lambda = -\lambda^{(2)} = \lambda^{(3)}$ (see (2.3)).

Generalization of the approach to the case of triaxial ellipsoids involves similar steps (summarized in [Appendix](#)), namely squaring each side of (2.4), averaging, and then

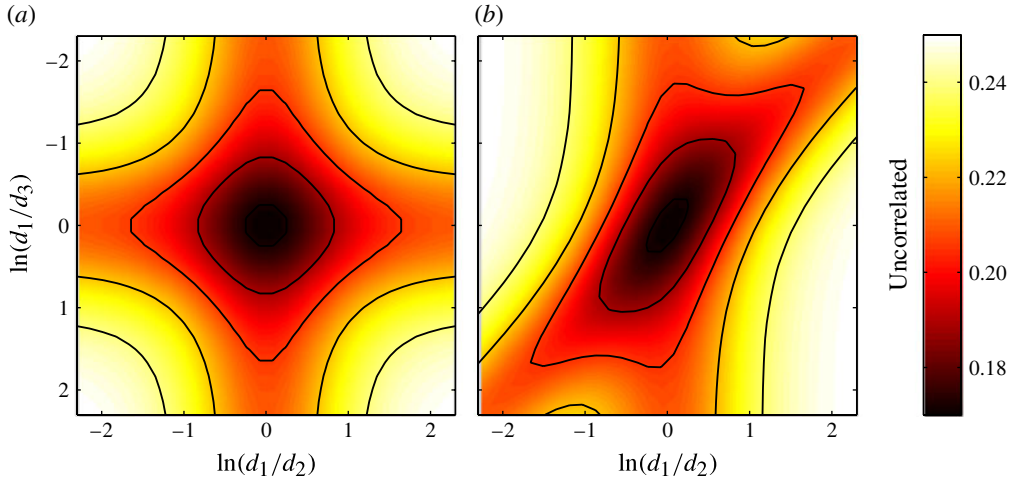


FIGURE 9. (Colour online) Variance of rate-of-change of two ellipsoid orientation vectors $\mathbf{p}^{(1)}$ and $\mathbf{p}^{(2)}$ as function of the two ratios of semi-axes length, when assuming independence of orientation vectors and turbulence velocity gradient tensor elements (from (4.2)). Contour lines go from 0.17 to 0.25 separated by 0.02: (a) $V^{(1)}$; (b) $V^{(2)}$.

using the assumed independence between the orientation vectors and the strain-rate and rotation-rate tensors to separate the averages. Then, isotropic tensor forms are assumed. As shown in [Appendix](#), the result is (see (A 14))

$$V_{SI}^{(i)} = \frac{1}{6} + \frac{1}{20} \sum_{k \neq i} (\lambda^{(k)})^2. \quad (4.2)$$

One recovers the result of Parsa *et al.* (2012) (4.1) using (4.2) for $d_2 = d_3$, i.e. $-\lambda^{(2)} = \lambda^{(3)} = \lambda$.

The results from assuming statistical independence between particle orientation and turbulent velocity gradient tensor are shown in figure 9. Comparing $V_{SI}^{(1)}$ with the results of DNS (see figure 3a), one can see significant differences. As already noted by Shin & Koch (2005), the assumption of independence leads to an over prediction of fluctuations, $V_{SI}^{(1)} \approx 0.26$, for rods (i.e. top-right corner), instead of $V^{(1)} \approx 0.09$ for DNS. Interestingly, the level of fluctuations predicted for disc-shaped particles (i.e. bottom-left quadrant) is close to that observed in DNS. Still, the assumption of statistical independence makes no difference between rods and discs. Similar conclusions can be reached about $V^{(2)}$ (figure 9b): DNS leads to marked differences between the cases $d_1/d_3 = (d_1/d_2)^{-1} \rightarrow 0$ and $d_1/d_3 = (d_1/d_2)^{-1} \rightarrow \infty$, whereas the assumption of statistical independence (4.2) does not lead to such differences.

4.2. Gaussian process

Next, we consider a linear Ornstein–Uhlenbeck process for the velocity gradient tensor according to

$$d\mathbf{A} = -\frac{1}{\tau_\eta} \mathbf{A} dt + \frac{1}{\tau_\eta^{3/2}} d\mathbf{W}. \quad (4.3)$$

The term \mathbf{W} is a tensorial delta-correlated noise that forces the equation. The relaxation term involves a simple time scale τ_η , i.e. the Kolmogorov time scale. In

this linear equation, the 1-point covariance structure of the velocity gradients \mathbf{A} is imposed by the covariance structure of the tensorial forcing term $d\mathbf{W}$, whereas the damping term $-\mathbf{A}/\tau_\eta$ enforces an exponential time correlation. To ensure isotropic statistics for \mathbf{A} , we use (see appendix A of Chevillard *et al.* (2008))

$$dW_{ij}(t) = D_{ijpq} dB_{pq}(t), \quad (4.4)$$

where \mathbf{B} is a tensorial Wiener process with independent elements, i.e. its increments are Gaussian, independent and satisfy

$$\langle dB_{pq} \rangle = 0 \quad \text{and} \quad \langle dB_{ij}(t) dB_{kl}(t) \rangle = 2 dt \delta_{ik} \delta_{jl}, \quad (4.5)$$

and the diffusion kernel is D_{ijpq} chosen as

$$D_{ijpq} = \frac{1}{3} \frac{3 + \sqrt{15}}{\sqrt{10} + \sqrt{6}} \delta_{ij} \delta_{pq} - \frac{\sqrt{10} + \sqrt{6}}{4} \delta_{ip} \delta_{jq} + \frac{1}{\sqrt{10} + \sqrt{6}} \delta_{iq} \delta_{jp}. \quad (4.6)$$

For such a process, one obtains in the stationary regime

$$\langle A_{ij}(t) A_{kl}(t + \tau) \rangle_{t \rightarrow \infty} = \frac{1}{\tau_\eta^2} e^{-|\tau|/\tau_\eta} \left[2\delta_{ik} \delta_{jl} - \frac{1}{2} \delta_{ij} \delta_{kl} - \frac{1}{2} \delta_{il} \delta_{jk} \right], \quad (4.7)$$

which is consistent with a covariance structure of a trace-free, homogeneous and isotropic tensor, exponentially correlated in time, and such that the variance of diagonal (respectively off-diagonal) elements is τ_η^{-2} (respectively $2\tau_\eta^{-2}$). Accordingly, the covariance structure of its symmetric part is

$$\langle S_{ij}(t) S_{kl}(t + \tau) \rangle_{t \rightarrow \infty} = \frac{1}{4\tau_\eta^2} e^{-|\tau|/\tau_\eta} [3\delta_{ik} \delta_{jl} - 2\delta_{ij} \delta_{kl} + 3\delta_{il} \delta_{jk}], \quad (4.8)$$

and

$$\langle \Omega_{ij}(t) \Omega_{kl}(t + \tau) \rangle_{t \rightarrow \infty} = \frac{5}{4\tau_\eta^2} e^{-|\tau|/\tau_\eta} [\delta_{ik} \delta_{jl} - \delta_{il} \delta_{jk}] \quad (4.9)$$

for the antisymmetric part. Remark that with this definition of τ_η , we get $\langle 2S_{pq} S_{pq} \rangle = \langle 2\Omega_{pq} \Omega_{pq} \rangle = \langle A_{pq} A_{pq} \rangle = 15/\tau_\eta^2 = \varepsilon/\nu$.

Simulation of this tensorial process generates a time series of $\mathbf{A}(t)$ which is used in the numerical solution of (2.2). The resulting variances of $\dot{\mathbf{p}}^{(1)}$ and $\dot{\mathbf{p}}^{(2)}$ are displayed in figure 10, top two plots (the bottom ones show predictions from a model discussed below in § 4.3). For the Gaussian process, it is seen that $V^{(1)}$ and $V^{(2)}$ depend only weakly on particle anisotropy, with values ranging only between 0.15 and 0.18. Further tests varying the forcing strength have been performed (not shown) and results are briefly commented upon in § 5.

Results for the flatness $F^{(i)}$ (equation (2.9)) are shown in figure 11 (top line). As can be seen, the Gaussian model (equation (4.3)) produces a flatness for the particle orientation rotation rates always close to two for all parameter values, at odds with DNS (cf. figure 4). The value of two can be exactly derived for spheres assuming orientation vectors independent from velocity gradients, themselves assumed Gaussian (see Appendix and (A 15)). While the observed trends are difficult to distinguish from numerical noise, they also clearly differ from the 5/3 value obtained from assuming

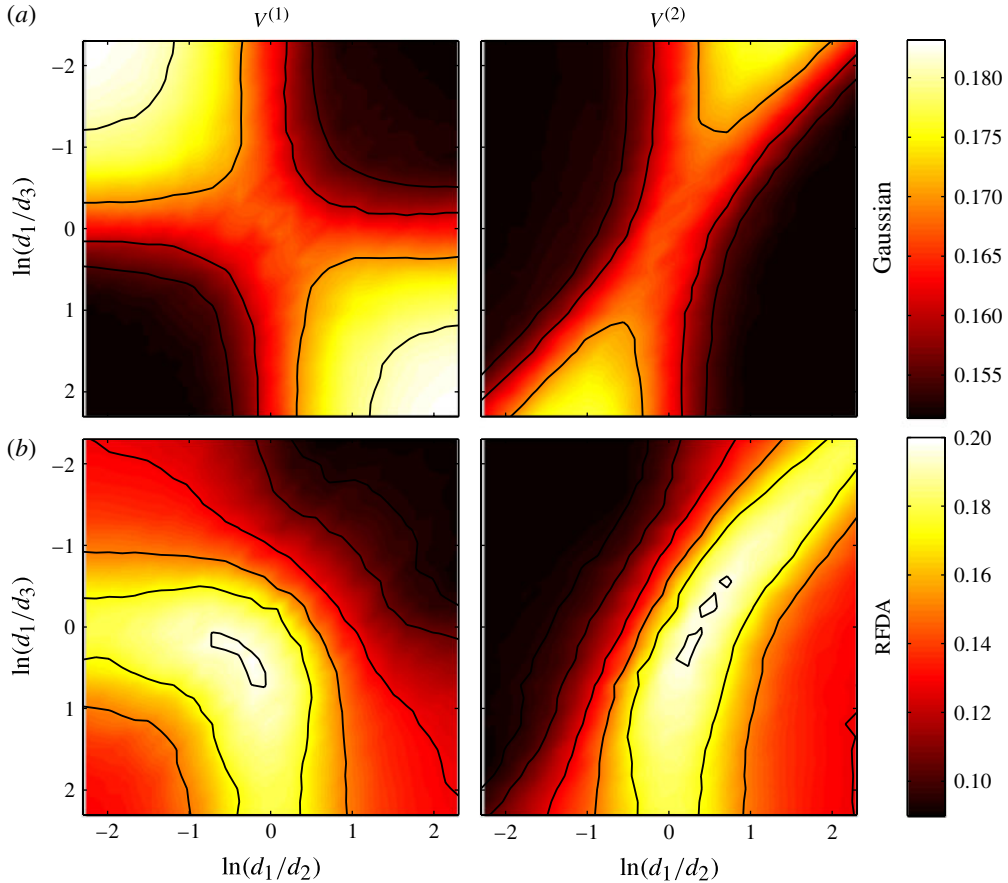


FIGURE 10. (Colour online) Variance of rate-of-change of the two ellipsoid orientation vectors $\mathbf{p}^{(1)}$ and $\mathbf{p}^{(2)}$ as function of the ratios of semi-axes length. (a) Gaussian stochastic model. (b) Results from RFDA Lagrangian stochastic model (see § 4.3). For the Gaussian case, contour lines correspond to values 0.155, 0.16, 0.17, 0.18, and for the RFDA case 0.09, 0.1, 0.12, 0.14, 0.16, 0.18, 0.2.

each element of \mathbf{p} to be a Gaussian independent variable. We are led to the conclusion that assuming statistically independent \mathbf{A} and $\mathbf{p}^{(i)}$, as well as a Gaussian process for \mathbf{A} with a correlation time scale of τ_η , gives a poor prediction of the rate of rotation of orientation vectors that has been observed in DNS.

Angular alignment trends will be discussed in the next section together with those of the RFDA model.

4.3. RFDA Lagrangian stochastic model

The Lagrangian model developed by Chevillard & Meneveau (2006) is given by the following non-dimensionalized, in units of the integral time scale T , stochastic differential equation

$$d\mathbf{A} = \left(-\mathbf{A}^2 + \frac{\text{Tr}(\mathbf{A}^2)}{\text{Tr}(\mathbf{C}_{\tau_\eta/T}^{-1})} \mathbf{C}_{\tau_\eta/T}^{-1} - \frac{\text{Tr}(\mathbf{C}_{\tau_\eta/T}^{-1})}{3} \mathbf{A} \right) dt + d\mathbf{W}. \quad (4.10)$$

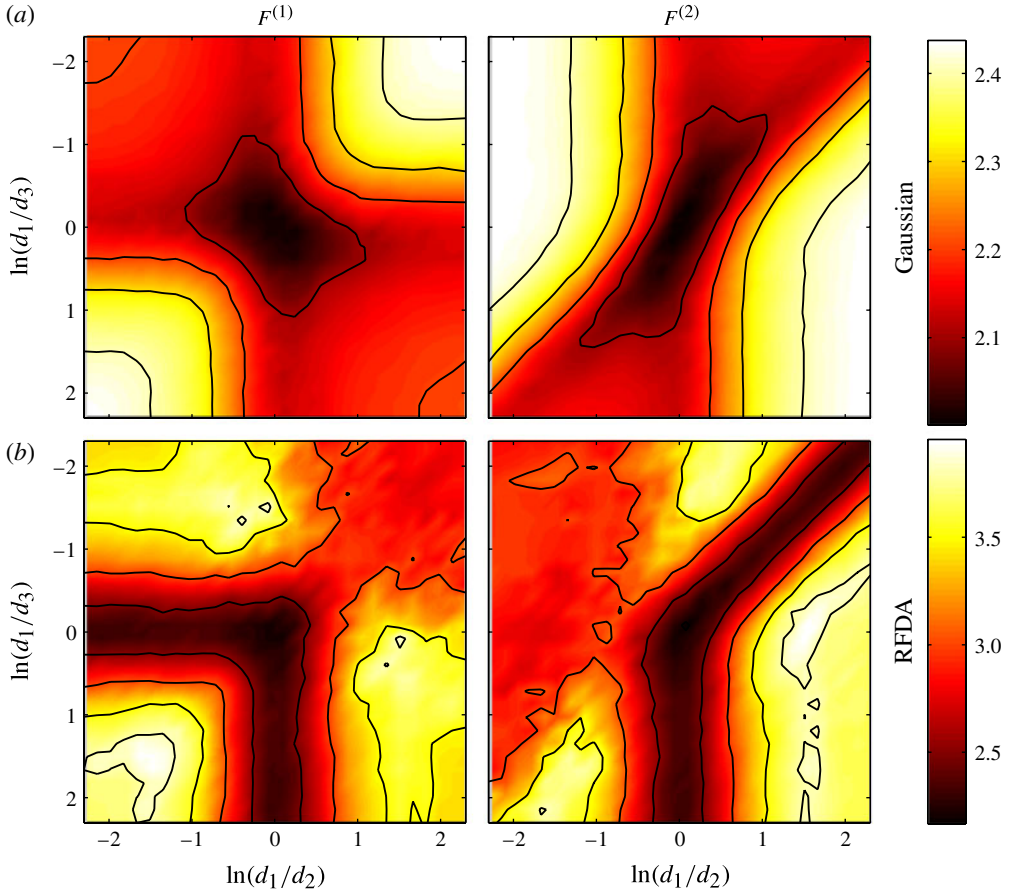


FIGURE 11. (Colour online) Flatness of rate-of-change of the two ellipsoid orientation vectors $\mathbf{p}^{(1)}$ and $\mathbf{p}^{(2)}$ as function of the two ratios of semi-axes length. (a) Gaussian stochastic model, for which the flatness is near two for any ellipsoidal aspect ratios. (b) Results from RFDA Lagrangian stochastic model (see § 4.3). For the Gaussian case, contour lines correspond to values 2.1, 2.2, 2.3, 2.4, and for the RFDA case, 2.2, 2.5, 3, 3.5, 3.8.

The *recent Cauchy–Green tensor* \mathbf{C}_{τ_η} , which arises after invoking the RFDA (Chevillard & Meneveau 2006) is written in terms of matrix exponentials as

$$\mathbf{C}_{\tau_\eta} = e^{\tau_\eta \mathbf{A}} e^{\tau_\eta \mathbf{A}^\top}, \quad (4.11)$$

where τ_η is (as before) the Kolmogorov time scale (see Chevillard *et al.* (2008) for additional details). The first three deterministic terms in (4.10) represent, respectively, the exact self-stretching term, and models for both pressure Hessian and viscous diffusion. The modelling is based on a Lagrangian–Eulerian change of variables coupled to the assumption that the Lagrangian pressure Hessian is an isotropic tensor. This differs from the assumption of the restricted Euler model in which the Eulerian pressure Hessian is assumed to be isotropic. Assuming that the velocity gradient is perfectly correlated during a time τ_K along the Lagrangian trajectory, while it is uncorrelated for longer time delays, leads to a closed-form expression for the model pressure Hessian in the form of matrix exponentials. The latter arise as solutions to

the kinematic equation for the deformation tensor. A similar derivation can be done for the Laplacian that arises in the viscous term. An analysis of expansions of the matrix exponentials is provided by Martins-Afonso & Meneveau (2010). The term \mathbf{W} is the same tensorial delta-correlated noise term that enters in the Gaussian process (equation (4.3)), it represents possible forcing effects, e.g. from neighbouring eddies.

The RFDA model has been shown to reproduce several important characteristics of the velocity gradient tensor, such as the preferential alignments of vorticity with the intermediate eigendirection of the strain and subtle temporal correlations (Chevillard & Meneveau 2011). It has thus a more complex covariance structure than that obtained from the Ornstein–Uhlenbeck process (equation (4.3)) and is more realistic (see Chevillard *et al.* 2008; Meneveau 2011). Yet, the model has some known limitations: as discussed further by Meneveau (2011), extensions to increasing Reynolds number (reducing τ_η/T below 10^{-2} or so) leads to unphysical tails in the velocity gradient p.d.f.s. Also, tests have shown that the process leads to small deviations between the variance of the strain-rate tensor and the rotation rate tensor, i.e. for $\tau_\eta/T = 0.1$, we obtain $\langle S_{ij}S_{ij} \rangle \approx 1.1\langle \Omega_{ij}\Omega_{ij} \rangle$. Further strengths and limitations of the model will be highlighted by comparing its predictions of particle orientation dynamics to DNS.

The process is simulated numerically using a standard second-order Runge–Kutta algorithm with a unique realization of the noise for each time step. The time series of $\mathbf{A}(t)$ generated by this process are, again, used in the solution of (2.2). The resulting variances of $\dot{\mathbf{p}}^{(1)}$ and $\dot{\mathbf{p}}^{(2)}$ are displayed in the bottom row of plots in figure 10. As can be seen, certain trends agree well with the results from the DNS. As opposed to the results from the Gaussian model, in the limit of rod-like particles ($d_1/d_2 = d_1/d_3 \gg 1$), the variance of $\dot{\mathbf{p}}^{(1)}$ decreases significantly. Alignment of $\mathbf{p}^{(1)}$ with the vorticity leads to a reduction of its rate of change. In the other limit ($d_1/d_2 = d_1/d_3 \ll 1$), however, the model predicts also some reduction of variance, unlike the DNS results. To better understand the origin of this result, the alignments of $\mathbf{p}^{(1)}$ with the strain-rate eigensystem will be quantified and compared with DNS.

In terms of the variance of $\dot{\mathbf{p}}^{(2)}$ shown in figure 10(d), we remark that there is good overall agreement between the model and DNS results: in the top left corner there is decreased variance, while towards the bottom-right corner the variance is generally higher. Nevertheless, a non-monotonic behaviour is observed here too, in which some decrease in variance towards $d_1/d_2 \gg 1$ can be observed.

In order to enable quantitative comparisons between DNS, the Gaussian model (equation (4.3)), and the RFDA model (equation (4.10)), we present sample results along the $d_1/d_2 = d_1/d_3$ line of parameters, i.e. the axisymmetric cases. Figure 12 shows the variance of $\dot{\mathbf{p}}^{(1)}$ for the DNS, Gaussian and RFDA models. The first two lines are very similar to the results shown in Parsa *et al.* (2012).

As far as the flatness factor is concerned (see figure 11, bottom row of contour plots), it is interesting to note that the RFDA model predicts qualitatively quite well the rather complex trends observed in DNS and displayed in figure 4. The main difference is that the flatness obtained from DNS is significantly higher than that obtained from the RFDA model. This could be also related to the fact that the RFDA model under predicts the flatness of the velocity gradient elements themselves (see Chevillard & Meneveau 2006). We gather the results for the flatness of the rotation rate of orientation vectors obtained from DNS, Gaussian and RFDA models in figure 12(b). Indeed, we see that the RFDA follows accurately the variations observed in DNS, but the overall value (around 6.5 for DNS and around 3 for RFDA) is not reproduced.

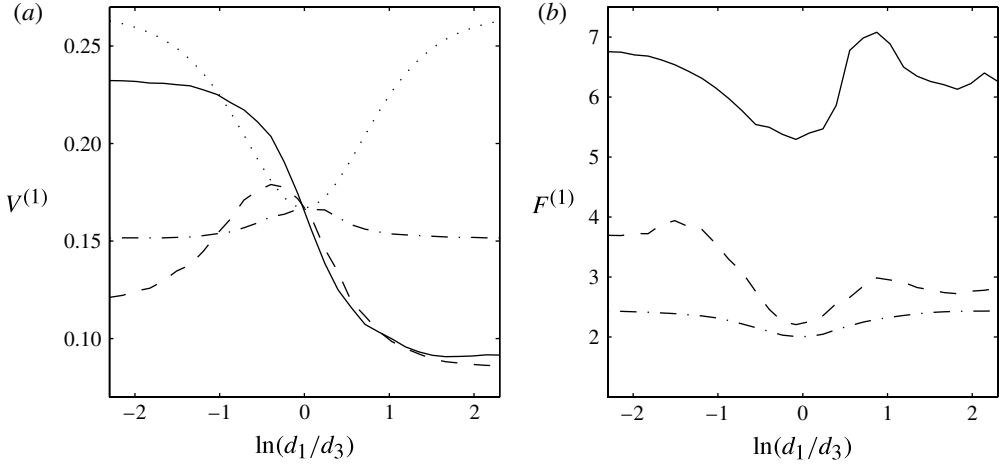


FIGURE 12. Variance (a) and flatness factor (b) of $\hat{\boldsymbol{p}}^{(1)}$ from DNS (solid line), the Gaussian model (dot-dashed) and the RFDA model (dashed line). We added also the prediction equation (4.2) (dotted line) assuming that $\boldsymbol{p}^{(i)}$ and velocity gradients are statistically independent.

Analysis of model predictions of orientations of $\boldsymbol{p}^{(1)}$ for axisymmetric particles (i.e. $d_1/d_2 = d_1/d_3$) with vorticity and strain-rate eigenvectors leads to the results shown in figures 13 and 14, for both Gaussian and RFDA models.

For the Gaussian model, no preferential alignments of $\boldsymbol{p}^{(1)}$ with vorticity can be observed. Results for alignment with the strain eigenframe show a strong preferential alignment of fibre-like particles with the eigenvector associated with the most extensive eigendirection, no preferential alignments with the intermediate eigendirection and preferential alignments of disc-like particles with the most contracting eigendirection. This numerical study reveals indeed, for this Gaussian model (equation (4.3)), a correlation between orientation vectors and velocity gradients, although of different nature as that observed in DNS: whereas preferential alignments of fibre-like particles with intermediate eigendirection and disc-like particle with most contracting one are found in DNS, Gaussian process only correctly predicts alignments of disc-like particles with most-contracting eigendirection and reveals non-realistic alignment properties of fibres.

More refined Gaussian processes have been proposed for velocity gradient statistics. For instance, Pumir & Wilkinson (2011) and Vincenzi (2013) have considered an Ornstein–Uhlenbeck process for \boldsymbol{A} with different correlation time scales for the symmetric and antisymmetric parts. This is more realistic, since it is known that in turbulence the correlation time scale for the rotation rate is significantly longer than that of the strain rate. Applying this stochastic model to the orientation dynamics of rods (i.e. with $d_1/d_2 = d_1/d_3 \rightarrow \infty$), Pumir & Wilkinson (2011) observe similarly a strong preferential alignment of \boldsymbol{p} with the strain eigenvector associated with the most positive eigenvalue. This differs from the observations in DNS (see figures 5 and 6), where \boldsymbol{p} is instead found to be preferentially aligned with the direction of vorticity. As argued before, such trends then have immediate implications on the particle rotation rates. These results and arguments highlight the importance of both the temporal and alignment structure of \boldsymbol{A} . Similar conclusions have been arrived at recently by Gustavsson, Einarsson & Mehlig (2013) who consider also the case of

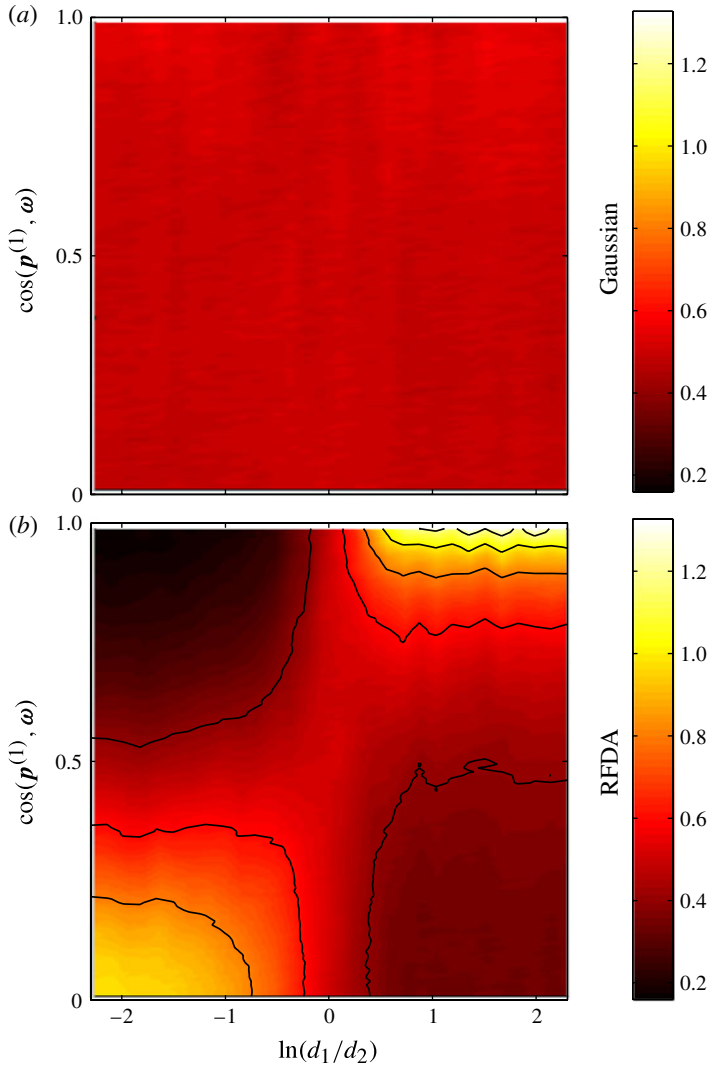


FIGURE 13. (Colour online) P.d.f. of the cosine of the angle between the vorticity direction $\hat{\omega}$ and the ellipsoid's major axis $\mathbf{p}^{(1)}$ for the axisymmetric case, as a function of the anisotropy parameter $\alpha = d_1/d_3 = d_1/d_2$. (a) Gaussian stochastic model (see § 4.2), for which the alignment appears flat, for any ellipsoidal aspect ratios. (b) Results from RFDA Lagrangian stochastic model. Contour lines correspond to values 0.4, 0.6, 0.8, 1, 1.2.

inertial axisymmetric particles and obtained analytical expressions for the rotation rate assuming an underlying Gaussian flow.

The alignments predicted by the RFDA model are significantly more realistic: as can be seen, for fibre-like particles ($d_1/d_2 \rightarrow \infty$), the model predicts strong alignment with vorticity (figure 13b). In the other limit, for disc-like particles, $\mathbf{p}^{(1)}$ in the model is preferentially perpendicular to the vorticity. That is to say, the vorticity is in the plane of the disc. Nevertheless, comparing in more detail with the DNS results in figure 5, it is evident that the model predicts a significantly broader (and weaker) alignment peak in the p.d.f. (see the different magnitudes given in colourbars). Hence, the alignment

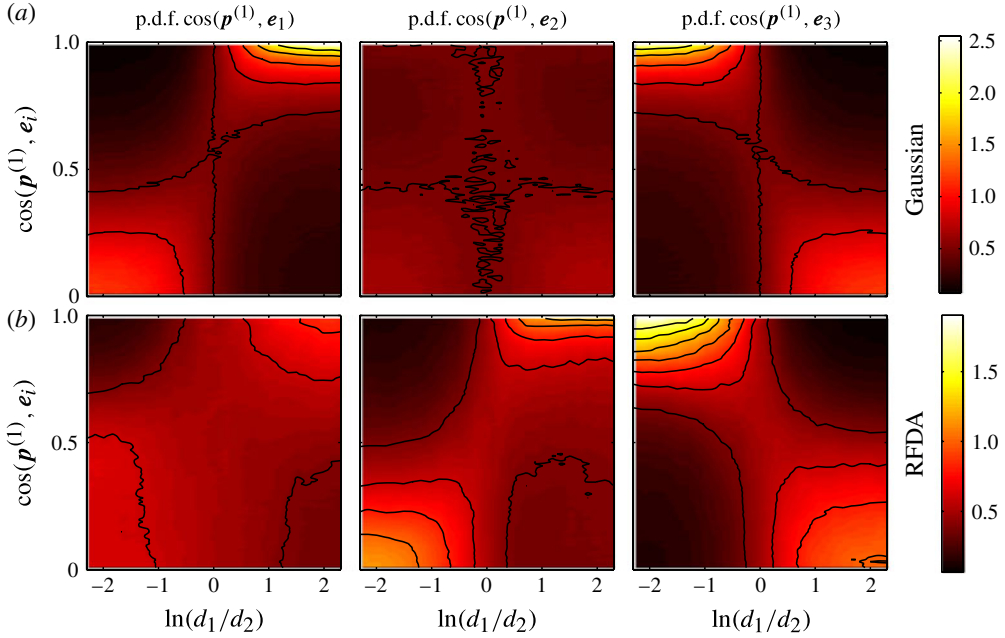


FIGURE 14. (Colour online) P.d.f. of the cosine of the angle between the strain-rate tensor eigendirections e_i and the ellipsoid's major axis $\mathbf{p}^{(1)}$ for the axisymmetric case ($\alpha = d_1/d_3 = d_1/d_2$), as a function of the anisotropy obtained from Gaussian (a) and RFDA (b) Lagrangian stochastic model. For the Gaussian case, contour lines correspond to values 0.5, 0.8, 1.2, 1.6, 2, and for the RFDA case, 0.4 0.6 0.8 1 1.2 1.4 1.6.

of the plane of the disc with vorticity is weaker in the model than in DNS, and as a result, the variance of $\dot{\mathbf{p}}^{(1)}$ for discs (perpendicular to the disc plane) is reduced compared with the DNS result, where the alignment of the disc plane with vorticity is much sharper.

For better comparisons among DNS, the Gaussian model and the RFDA model, we present vorticity alignment result for three values of d_1/d_3 along the $d_1/d_2 = d_1/d_3$ axisymmetry line. Figure 15 shows the p.d.f. of the cosine between $\mathbf{p}^{(1)}$ and the vorticity for the DNS, Gaussian and RFDA model. We indeed see that, whereas the Gaussian model does not predict any preferential alignments, the RFDA model predicts correct trends. However, the preferential alignment (when $d_1/d_3 \rightarrow \infty$) and even more the orthogonality (when $d_1/d_3 \rightarrow 0$) are weaker than those observed in DNS.

The alignments of $\mathbf{p}^{(1)}$ with each of the strain-rate eigenvectors are also established using the p.d.f. of the respective angle cosines. Results are shown in figure 14 (bottom line). Overall, the results from the RFDA model for the alignments of the orientation vectors with the strain-rate eigenframe appears to be quite realistic, both in trends and amplitudes (compare figure 6 and the bottom line of figure 14). As in DNS, the strongest alignment trend seems to be that for disc-like particles to align with the most contracting eigendirection. As observed previously, rod-like particles tend to align well with the intermediate eigenvectors, while disc-like particles show preponderance of perpendicular orientation with regards to the intermediate eigenvector. Again, this is consistent with the trends with vorticity. Interestingly, alignment trends with the most stretching eigendirection appear very weak, almost random, as in the DNS.

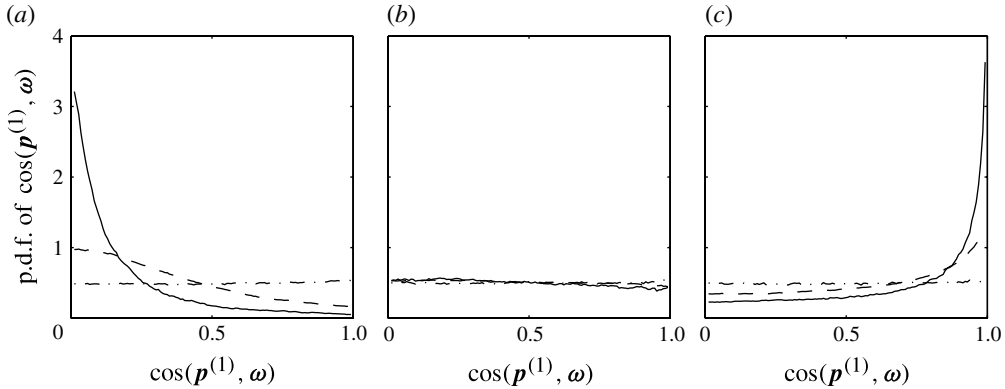


FIGURE 15. P.d.f.s of the cosine of the angle between vorticity and $\mathbf{p}^{(1)}$, for three values of α along the $d_1/d_2 = d_1/d_3$ line (the axisymmetric cases). Results from DNS (solid line), Gaussian model (dot-dashed) and RFDA model (dashed line) are shown: (a) $d_1/d_3 = 0.1$; (b) $d_1/d_3 = 1$; (c) $d_1/d_3 = 10$.

Finally, we have also considered the orientation statistics of the vector $\mathbf{p}^{(2)}$ with respect to vorticity and strain-rate eigendirections, along the $d_1/d_2 = (d_1/d_3)^{-1}$ line. The results (not shown) are very similar to those displayed in figures 13 and 14, as it was observed for the DNS (figures 7 and 8).

5. Conclusions

In this study, the orientation dynamics of anisotropic particles in isotropic turbulence has been examined using DNS and some stochastic models. We have generalized a recent analysis for axisymmetric ellipsoids (Parsa *et al.* 2012) to the case of general, triaxial–ellipsoidal tracer particles, without the assumption of axisymmetry. The underlying evolution equation that has been used was developed using asymptotic analysis for inertia-free local linear flow by Junk & Illner (2007). The analysis is valid for small particles which are smaller than the turbulent flow’s Kolmogorov scale.

The orientation dynamics are characterized by the rates of rotation of the particle’s two perpendicular orientation unit vectors, their variances and flatness, as well as with distribution functions of the orientation with respect to the flow’s vorticity and strain-rate eigenvector directions. Measurements based on Lagrangian tracking in DNS of isotropic turbulence show that triaxial ellipsoids that are very long in one direction, very thin in another and of intermediate size in the third direction exhibit reduced rotation rates that are similar to those of rods in the ellipsoid’s longest direction. Conversely, they exhibit increased rotation rates that are similar to those of axisymmetric discs in the direction of their smallest thickness.

In comparing DNS results with various models and assumptions, we find that they differ significantly from the case when the particle orientations are assumed to be statistically independent from the velocity gradient tensor. DNS results also differ significantly from results obtained when the velocity gradient tensor is modelled using an Ornstein–Uhlenbeck process with Gaussian statistics, with a forcing strength such that the velocity gradient standard deviation is on the same order of magnitude as the inverse of the temporal correlation time of the process. In that case, the velocity gradient tensor displays no preferred vorticity–strain-rate tensor alignments. Further tests (not shown) with the Ornstein–Uhlenbeck process have been performed, by

varying the strength of the forcing. It is observed that when the forcing strength is reduced from the baseline (high) values (i.e. $\sim 1/\tau_\eta^{3/2}$) to values of the order of $1/T^{3/2}$ (or unity, when using units of T , as was the case for the RFDA model) while maintaining the correlation time fixed at τ_η , then the results tend to those obtained assuming statistical independence among orientation vectors and the velocity gradient tensor. The fact that the two approaches lead to the same result can be understood as follows: the dimensionless quantities $V^{(i)}$ may only depend on dimensionless parameters. One of these is, e.g., $\theta = \tau_\eta \langle \Omega_{ij} \Omega_{ij} \rangle^{1/2}$, a combination of the process correlation time scale τ_η and the velocity gradient variance. Hence, reducing the forcing strength in the Gaussian process, i.e. letting $\langle \Omega_{ij} \Omega_{ij} \rangle \rightarrow 0$ while keeping τ_η fixed implies $\theta \rightarrow 0$. This same limit may be achieved by keeping the variance fixed but reducing the correlation time scale $\tau_\eta \rightarrow 0$. When the correlation time scale of the velocity gradient tensor tends to zero, one expects the same results as assuming statistical independence between the orientation vectors and the velocity gradient tensor.

DNS results are also compared with a stochastic model for the velocity gradient tensor in which the pressure and viscous effects are modelled based on the RFDA. We remark that in the RFDA model, the nonlinear terms cause a large velocity gradient variance (finite θ) even when the forcing strength is weak. Thus, in the RFDA model the variance and the correlation time are linked and cannot be controlled independently as they can be in the Ornstein–Uhlenbeck model. Unlike the Gaussian linear model, the RFDA-based stochastic model accurately predicts the reduction in rotation rate in the longest direction of triaxial ellipsoids. This is due to the fact that this direction aligns well with the flow’s vorticity, with its rotation perpendicular to the vorticity thus being reduced. For disc-like particles, or in directions perpendicular to the longest direction in triaxial particles, the model predicts smaller rotation rates than those observed in DNS (although still larger than for rods). This behaviour has been explained based on the probability of vorticity orientation with the most contracting strain-rate eigendirection. In DNS, this alignment is very likely (sharp peak in the p.d.f.), whereas the peak in the p.d.f. predicted by the model is more diffused. Furthermore, the RFDA model falls short at reproducing the high flatness of the rotation rate amplitude (i.e. $p_i p_i$, see figure 12*b*), although trends (exceeding the Gaussian values) are consistent. The under-prediction of flatness is likely due to the fact that the model does not reproduce the intermittent peak values of the velocity gradient components themselves (see Chevillard & Meneveau 2006) in which the high-intensity tails of the velocity gradient elements can be seen to fall off faster than those in DNS. Present results point to the need for further improvements in stochastic Lagrangian models for the velocity gradient tensor. Specifically, a model that predicts a sharper alignment between vorticity in a plane perpendicular to the most contracting strain-rate eigendirection would be expected to lead to a more accurate prediction of the increased rotation rates of discs.

The deformation and breakup of viscous drops in shear flows are greatly affected by the Lagrangian properties of fluid velocity gradients (Stone 1994). In some cases, it is possible to assume droplets are of ellipsoidal shape, as was done for example by Mosler & Shaqfeh (1997) and Maffettone & Minale (1998), or even allowing for more non-trivial shape deformations (Cristini *et al.* 2003). In either case, non-trivial correlations among the drop deformations and the strain eigendirections and vorticity of the flow suggest that turbulence will affect the rotation (tumbling) rates of deforming particles differently than is the case for rigid particles. Exploration of the RFDA model in the context of deforming particles is left for future studies.

Acknowledgements

The authors thank Emmanuel L ev eque for providing the authors with the Lagrangian time series of velocity gradient tensor from DNS, B. Castaing and A. Prosperetti for fruitful discussions, D. Bartolo on plotting issues. C.M. thanks the Laboratoire de Physique de l' cole Normale Sup erieure de Lyon for their hospitality during a sabbatical stay and the US National Science Foundation (grant # CBET-1033942) for support of turbulence research. We also thank the PSMN (ENS Lyon) for computational resources.

Appendix. Calculation of the variance of rotation rates for the independent case

In this section, we present the calculation of $V^{(i)} = \langle \dot{\mathbf{p}}^{(i)} \cdot \dot{\mathbf{p}}^{(i)} \rangle$ for the case when it is assumed that $\mathbf{p}^{(i)}$, for any $i = 1, 2, 3$, is statistically independent of the strain-rate and rotation tensors. We furthermore assume that each $\mathbf{p}^{(i)}$ is an isotropic vector, and recall that the set of vectors $(\mathbf{p}^{(1)}, \mathbf{p}^{(2)}, \mathbf{p}^{(3)})$ is an orthonormal basis. For this purpose, each side of the Junke–Illner equation (see (2.4)) is squared and averaged:

$$\begin{aligned} \langle \dot{\mathbf{p}}_n^{(i)} \dot{\mathbf{p}}_n^{(i)} \rangle &= \left\langle \left(\Omega_{nj} p_j^{(i)} + \sum_{k,m} \epsilon_{ikm} \lambda^{(m)} p_n^{(k)} p_q^{(k)} S_{ql} p_l^{(i)} \right) \right. \\ &\quad \left. \times \left(\Omega_{ng} p_g^{(i)} + \sum_{a,b} \epsilon_{iab} \lambda^{(b)} p_n^{(a)} p_r^{(a)} S_{rs} p_s^{(i)} \right) \right\rangle. \end{aligned} \quad (\text{A } 1)$$

Expanding and using the assumption of statistical independence between \mathbf{p} , \mathbf{S} and Ω , the following expressions must be evaluated:

$$\langle \Omega_{nj} p_j^{(i)} \Omega_{ng} p_g^{(i)} \rangle = \langle \Omega_{nj} \Omega_{ng} \rangle \langle p_j^{(i)} p_g^{(i)} \rangle, \quad (\text{A } 2)$$

$$2 \left\langle \Omega_{nj} p_j^{(i)} \sum_{a,b} \epsilon_{iab} \lambda^{(b)} p_n^{(a)} p_r^{(a)} S_{rs} p_s^{(i)} \right\rangle = 2 \langle \Omega_{nj} S_{rs} \rangle \sum_{a,b} \epsilon_{iab} \lambda^{(b)} \langle p_j^{(i)} p_s^{(i)} p_n^{(a)} p_r^{(a)} \rangle, \quad (\text{A } 3)$$

and

$$\begin{aligned} &\left\langle \sum_{k,m} \epsilon_{ikm} \lambda^{(m)} p_n^{(k)} p_q^{(k)} S_{ql} p_l^{(i)} \sum_{a,b} \epsilon_{iab} \lambda^{(b)} p_n^{(a)} p_r^{(a)} S_{rs} p_s^{(i)} \right\rangle \\ &= \langle S_{ql} S_{rs} \rangle \sum_{k,m} \sum_{a,b} \epsilon_{ikm} \epsilon_{iab} \lambda^{(m)} \lambda^{(b)} \langle p_n^{(k)} p_n^{(a)} p_q^{(k)} p_r^{(a)} p_l^{(i)} p_s^{(i)} \rangle. \end{aligned} \quad (\text{A } 4)$$

The set of vectors $(\mathbf{p}^{(1)}, \mathbf{p}^{(2)}, \mathbf{p}^{(3)})$ is an orthonormal basis, thus

$$p_n^{(k)} p_n^{(a)} = \delta_{ka}. \quad (\text{A } 5)$$

This implies that (A 4) simplifies to

$$\begin{aligned} &\left\langle \sum_{k,m} \epsilon_{ikm} \lambda^{(m)} p_n^{(k)} p_q^{(k)} S_{ql} p_l^{(i)} \sum_{a,b} \epsilon_{iab} \lambda^{(b)} p_n^{(a)} p_r^{(a)} S_{rs} p_s^{(i)} \right\rangle \\ &= \langle S_{ql} S_{rs} \rangle \sum_{m,b,k} \epsilon_{ikm} \epsilon_{ikb} \lambda^{(m)} \lambda^{(b)} \langle p_q^{(k)} p_r^{(k)} p_l^{(i)} p_s^{(i)} \rangle. \end{aligned} \quad (\text{A } 6)$$

We can see that the average of $|\dot{\mathbf{p}}^{(i)}|^2$ (equation (A 1)) depends only on the statistics of velocity gradients and second and fourth moments of orientation vector components. Assumption of isotropy for the unit vectors $\dot{\mathbf{p}}^{(i)}$ implies that

$$\langle p_j^{(i)} p_g^{(i)} \rangle = \frac{1}{3} \delta_{jg}, \quad (\text{A } 7)$$

$$\langle p_q^{(k)} p_r^{(k)} p_l^{(i)} p_s^{(i)} \rangle = A^{(k,i)} \delta_{qr} \delta_{ls} + B^{(k,i)} \delta_{ql} \delta_{rs} + C^{(k,i)} \delta_{qs} \delta_{rl}. \quad (\text{A } 8)$$

From there it is easily seen that (A 3) gives no contributions since any contractions of $\Omega_{nj} S_{rs}$ vanish. The three remaining unknown coefficients that enter in the evaluation of (A 6) may be found by specifying particular values. For instance, the index contraction $q = r$ and $l = s$ yields

$$\langle p_q^{(k)} p_q^{(k)} p_l^{(i)} p_l^{(i)} \rangle = \langle 1 \times 1 \rangle = 1 = 9A^{(k,i)} + 3B^{(k,i)} + 3C^{(k,i)}. \quad (\text{A } 9)$$

Inspecting (A 6), we note that terms in the sum such that $k = i$ give no contribution because of the $\epsilon_{ikm} \epsilon_{ikb}$. Thus, we consider $k \neq i$. In this case, the contraction $q = l$ and $r = s$ yields

$$0 = 3A^{(k,i)} + 9B^{(k,i)} + 3C^{(k,i)}, \quad (\text{A } 10)$$

and the contraction $q = s$ and $r = l$ yields

$$0 = 3A^{(k,i)} + 3B^{(k,i)} + 9C^{(k,i)}. \quad (\text{A } 11)$$

Solving these equations yields in the case $k \neq i$

$$A^{(k,i)} = \frac{2}{15} \quad \text{and} \quad B^{(i,a)} = C^{(i,a)} = -\frac{1}{30}. \quad (\text{A } 12)$$

Finally, simplifying (A 2) with (A 7) and contracting the isotropic form (A 8) with $\langle S_{ql} S_{rs} \rangle$, we obtain

$$\langle |\dot{\mathbf{p}}^{(i)}|^2 \rangle = \frac{1}{3} \langle \Omega_{pq} \Omega_{pq} \rangle + \frac{1}{10} \langle S_{pq} S_{pq} \rangle \sum_{m,b,k \neq i} \epsilon_{ikm} \epsilon_{ikb} \lambda^{(m)} \lambda^{(b)}. \quad (\text{A } 13)$$

Using the isotropic relations $\langle \Omega_{pq} \Omega_{pq} \rangle = \langle S_{pq} S_{pq} \rangle$ and normalizing the former relation by $2 \langle \Omega_{pq} \Omega_{pq} \rangle = \varepsilon/\nu$, we get the following functional forms for the fluctuation of rotation rate variances:

$$V_{SI}^{(i)} = \frac{1}{6} + \frac{1}{20} \sum_{k \neq i} (\lambda^{(k)})^2. \quad (\text{A } 14)$$

If furthermore the statistics of \mathbf{A} are assumed Gaussian (as in § 4.2), it is also possible to derive exactly the value for the flatness, although the calculation is more tedious. For the particular case of spheres, i.e. $d_1 = d_2 = d_3$ or $\lambda^{(i)} = 0$, the dynamics is rather simple since $\dot{p}_n^{(i)} = \Omega_{nj} p_j^{(i)}$. Assuming that $\mathbf{p}^{(i)}$ is isotropic and independent on \mathbf{A} , we easily obtain $\langle |\dot{\mathbf{p}}^{(i)}|^4 \rangle = [\langle \text{tr}^2 \Omega \Omega^\top \rangle + 2 \langle \text{tr}(\Omega \Omega^\top)^2 \rangle] / 15$. For isotropic, homogeneous and trace-free Gaussian velocity gradient tensors, we obtain $\langle \text{tr}^2 \Omega \Omega^\top \rangle = 5 \langle \text{tr} \Omega \Omega^\top \rangle^2 / 3$ and $\langle \text{tr}(\Omega \Omega^\top)^2 \rangle = 5 \langle \text{tr} \Omega \Omega^\top \rangle^2 / 6$. Since, $\langle |\dot{\mathbf{p}}^{(i)}|^2 \rangle = \langle \text{tr} \Omega \Omega^\top \rangle / 3$, we finally obtain

$$F_{SI}^{(i)}(1, 1) = 2. \quad (\text{A } 15)$$

REFERENCES

- ASHURST, W. T., KERSTEIN, R., KERR, R. & GIBSON, C. 1987 Alignment of vorticity and scalar gradient with the strain rate in simulated Navier–Stokes turbulence. *Phys. Fluids* **30**, 2343–2353.
- BERNSTEIN, O. & SHAPIRO, M. 1994 Direct determination of the orientation distribution function of cylindrical particles immersed in laminar and turbulent shear flows. *J. Aerosol Sci.* **25**, 113–136.
- BIFERALE, L., CHEVILLARD, L., MENEVEAU, C. & TOSCHI, F. 2007 Multiscale model of gradient evolution in turbulent flows. *Phys. Rev. Lett.* **98**, 214501.
- BRETHERTON, F. P. 1962 The motion of rigid particles in a shear flow at low Reynolds number. *J. Fluid Mech.* **14**, 284–304.
- BRUNK, B. K., KOCH, D. L. & LION, L. W. 1998 A model for alignment between microscopic rods and vorticity. *J. Fluid Mech.* **364**, 81–113.
- CANTWELL, B. J. 1992 Exact solution of a restricted Euler equation for the velocity gradient tensor. *Phys. Fluids A* **4**, 782–793.
- CHERTKOV, M., PUMIR, A. & SHRAIMAN, B. I. 1999 Lagrangian tetrad dynamics and the phenomenology of turbulence. *Phys. Fluids* **11**, 2394–2410.
- CHEVILLARD, L., MENEVEAU, C., BIFERALE, L. & TOSCHI, F. 2008 Modelling the pressure Hessian and viscous Laplacian in turbulence: comparisons with direct numerical simulation and implications on velocity gradient dynamics. *Phys. Fluids* **20**, 101504.
- CHEVILLARD, L. & MENEVEAU, C. 2006 Lagrangian dynamics and statistical geometric structure of turbulence. *Phys. Rev. Lett.* **97**, 174501.
- CHEVILLARD, L. & MENEVEAU, C. 2007 Intermittency and universality in a Lagrangian model of velocity gradients in three-dimensional turbulence. *C. R. Méc.* **335**, 187–193.
- CHEVILLARD, L. & MENEVEAU, C. 2011 Lagrangian time correlations of vorticity alignments in isotropic turbulence: observations and model predictions. *Phys. Fluids* **23**, 101704.
- CRISTINI, V., BLAWZDZIEWICZ, J. B., LOEWENBERG, M. & COLLINS, L. R. 2003 Breakup in stochastic Stokes flows: sub-Kolmogorov drops in isotropic turbulence. *J. Fluid Mech.* **492**, 231–250.
- GIERSZEWSKI, P. J. & CHAFFEY, C. E. 1978 Rotation of an isolated triaxial ellipsoid suspended in slow viscous flow. *Canad. J. Phys.* **56**, 6–11.
- GIRIMAJI, S. S. & POPE, S. B. 1990a A diffusion model for velocity gradients in turbulence. *Phys. Fluids A* **2**, 242–256.
- GIRIMAJI, S. S. & POPE, S. B. 1990b Material element deformation in isotropic turbulence. *J. Fluid Mech.* **220**, 427–458.
- GONZALEZ, M. 2009 Kinematic properties of passive scalar gradient predicted by a stochastic Lagrangian model. *Phys. Fluids* **21**, 055104.
- GUSTAVSSON, K., EINARSSON, J. & MEHLIG, B. 2013 Tumbling of small axisymmetric particles in random and turbulent flows. Preprint arXiv: [1305.1822](https://arxiv.org/abs/1305.1822).
- HATER, T., HOMANN, H. & GRAUER, R. 2011 Lagrangian model for the evolution of turbulent magnetic and passive scalar fields. *Phys. Rev. E* **83**, 017302.
- HINCH, E. J. & LEAL, L. G. 1979 Rotation of small non-axisymmetric particles in a simple shear flow. *J. Fluid Mech.* **92**, 591.
- JEFFERY, G. B. 1922 The motion of ellipsoidal particles immersed in a viscous fluid. *Proc. R. Soc. Lond. A* **102**, 161–179.
- JEONG, E. & GIRIMAJI, S. S. 2003 Velocity-gradient dynamics in turbulence: effect of viscosity and forcing. *Theor. Comput. Fluid Dyn.* **16**, 421–432.
- JUNK, M. & ILLNER, R. 2007 A new derivation of Jeffery’s equation. *J. Math. Fluid Mech.* **9**, 455–488.
- KOCH, D. L. & SUBRAMANIAN, G. R. 2011 Collective hydrodynamics of swimming microorganisms: living fluids. *Annu. Rev. Fluid Mech.* **434**, 637–659.
- LARSON, R. G. 1999 *The Structure and Rheology of Complex Fluid*. Oxford University Press.
- LI, Y. 2011 Small-scale intermittency and local anisotropy in turbulent mixing with rotation. *J. Turbul.* **12**, N38.

- LUNDELL, F., SODERBERG, D. L. & ALFREDSSON, H. P. 2011 Fluid mechanics of papermaking. *Annu. Rev. Fluid Mech.* **43**, 195.
- MAFFETTONE, P. L. & MINALE, M. 1998 Equation of change for ellipsoidal drops in viscous flow. *J. Non-Newtonian Fluid Mech.* **78**, 227–241.
- MARTINS-AFONSO, M. & MENEVEAU, C. 2010 Recent fluid deformation closure for velocity gradient tensor dynamics in turbulence: timescale effects and expansions. *Physica D* **239**, 1241–1250.
- MENEVEAU, C. 2011 Lagrangian dynamics and models of the velocity gradient tensor in turbulent flows. *Annu. Rev. Fluid Mech.* **43**, 219–245.
- MORTENSEN, P. H., ANDERSON, H. I., GILLISSEN, J. J. J. & BOERSMA, B. J. 2008 Dynamics of prolate ellipsoidal particles in a turbulent channel flow. *Phys. Fluids* **20**, 093302.
- MOSLER, A. B. & SHAQFEH, E. S. G. 1997 Drop breakup in the flow through fixed beds via stochastic simulation in model Gaussian fields. *Phys. Fluids* **9**, 3209.
- NASO, A., PUMIR, A. & CHERTKOV, M. 2007 Statistical geometry in homogeneous and isotropic turbulence. *J. Turbul.* **8**, N. 39.
- NEWSOM, R. K. & BRUCE, C. W. 1998 Orientational properties of fibrous aerosols in atmospheric turbulence. *J. Aerosol Sci.* **29**, 773–797.
- PARSA, S., CALZAVARINI, E., TOSCHI, F. & VOTH, G. A. 2012 Rotation rate of rods in turbulent fluid flow. *Phys. Rev. Lett.* **109**, 134501.
- PEDLEY, T. J. & KESSLER, J. O. 1992 Hydrodynamic phenomena in suspensions of swimming microorganisms. *Annu. Rev. Fluid Mech.* **24**, 313–358.
- PINSKY, M. B. & KHAIN, A. P. 1998 Some effects of cloud turbulence on water–ice and ice–ice collisions. *Atmos. Res.* **47–48**, 69–86.
- PUMIR, A. & WILKINSON, M. 2011 Orientation statistics of small particles in turbulence. *New J. Phys.* **13**, 0930306.
- SAINTILLAN, D. & SHELLEY, M. J. 2007 Orientational order and instabilities in suspensions of self-locomoting rods. *Phys. Rev. Lett.* **99**, 058102.
- SHIN, M. & KOCH, D. L. 2005 Rotational and translational dispersion of fibres in isotropic turbulent flows. *J. Fluid Mech.* **540**, 143–173.
- STONE, H. A. 1994 Dynamics of drop deformation and breakup in viscous fluids. *Annu. Rev. Fluid Mech.* **26**, 65–102.
- VINCENZI, D. 2013 Orientation of non-spherical particles in an axisymmetric random flow. *J. Fluid Mech.* **719**, 465–487.
- WILKINSON, M. & KENNARD, H. R. 2012 A model for alignment between microscopic rods and vorticity. *J. Phys. A: Math. Theor.* **45**, 455502.
- YARIN, A. L., GOTTLIEB, O. & ROISMAN, I. V. 1997 Chaotic rotation of triaxial ellipsoids in simple shear flow. *J. Fluid Mech.* **340**, 83–100.
- ZHANG, H., AHMADI, G., FAN, F. G. & MCLAUGHLIN, J. B. 2001 Ellipsoidal particles transport and deposition in turbulent channel flows. *Intl. J. Multiphase Flow* **27**, 971–1009.
- ZIMMERMANN, R., GASTEUIL, Y., BOURGOIN, M., VOLK, R., PUMIR, A. & PINTON, J.-F. 2011 Rotational intermittency and turbulence induced lift experienced by large particles in a turbulent flow. *Phys. Rev. Lett.* **106**, 154501.